



**HAL**  
open science

## Are the orbital poles of binary stars in the solar neighbourhood anisotropically distributed?

J.-L. Agati, D. Bonneau, A. Jorissen, E. Soulié, S. Udry, P. Verhas, J. Dommagnet

► **To cite this version:**

J.-L. Agati, D. Bonneau, A. Jorissen, E. Soulié, S. Udry, et al.. Are the orbital poles of binary stars in the solar neighbourhood anisotropically distributed?. *Astronomy and Astrophysics - A&A*, 2015, 574, pp.A6. 10.1051/0004-6361/201323056 . cea-01290090

**HAL Id: cea-01290090**

**<https://cea.hal.science/cea-01290090>**

Submitted on 17 Mar 2016

**HAL** is a multi-disciplinary open access archive for the deposit and dissemination of scientific research documents, whether they are published or not. The documents may come from teaching and research institutions in France or abroad, or from public or private research centers.

L'archive ouverte pluridisciplinaire **HAL**, est destinée au dépôt et à la diffusion de documents scientifiques de niveau recherche, publiés ou non, émanant des établissements d'enseignement et de recherche français ou étrangers, des laboratoires publics ou privés.

# Are the orbital poles of binary stars in the solar neighbourhood anisotropically distributed?★

J.-L. Agati<sup>1</sup>, D. Bonneau<sup>2</sup>, A. Jorissen<sup>3</sup>, E. Soulié<sup>4</sup>, S. Udry<sup>5</sup>, P. Verhas<sup>6</sup>, and J. Dommanget<sup>†,7</sup>

<sup>1</sup> 13 rue Beyle Stendhal, 38000 Grenoble, France

<sup>2</sup> Laboratoire Lagrange, UMR 7293, Univ. Nice Sophia-Antipolis, CNRS, Observatoire de la Côte d'Azur, 06300 Nice, France  
e-mail: daniel.bonneau@oca.eu

<sup>3</sup> Institut d'Astronomie et d'Astrophysique, Université Libre de Bruxelles, CP 226, Boulevard du Triomphe, 1050 Brussels, Belgium

<sup>4</sup> CEA/Saclay, DSM, 91191 Gif-sur-Yvette Cedex, France

<sup>5</sup> Observatoire de Genève, Chemin des Maillettes, 1290 Sauverny, Suisse

<sup>6</sup> 251 vieille rue du Moulin, 1180 Brussels, Belgium

<sup>7</sup> Observatoire Royal de Belgique, Avenue Circulaire 3, 1180 Bruxelles, Belgique

Received 15 November 2013 / Accepted 30 October 2014

## ABSTRACT

We test whether or not the orbital poles of the systems in the solar neighbourhood are isotropically distributed on the celestial sphere. The problem is plagued by the ambiguity on the position of the ascending node. Of the 95 systems closer than 18 pc from the Sun with an orbit in the 6th Catalogue of Orbits of Visual Binaries, the pole ambiguity could be resolved for 51 systems using radial velocity collected in the literature and CORAVEL database or acquired with the HERMES/Mercator spectrograph. For several systems, we can correct the erroneous nodes in the 6th Catalogue of Orbits and obtain new combined spectroscopic/astrometric orbits for seven systems [WDS 01083+5455Aa,Ab; 01418+4237AB; 02278+0426AB (SB2); 09006+4147AB (SB2); 16413+3136AB; 17121+4540AB; 18070+3034AB]. We used of spherical statistics to test for possible anisotropy. After ordering the binary systems by increasing distance from the Sun, we computed the false-alarm probability for subsamples of increasing sizes, from  $N = 1$  up to the full sample of 51 systems. Rayleigh-Watson and Beran tests deliver a false-alarm probability of 0.5% for the 20 systems closer than 8.1 pc. To evaluate the robustness of this conclusion, we used a jackknife approach, for which we repeated this procedure after removing one system at a time from the full sample. The false-alarm probability was then found to vary between 1.5% and 0.1%, depending on which system is removed. The reality of the deviation from isotropy can thus not be assessed with certainty at this stage, because only so few systems are available, despite our efforts to increase the sample. However, when considering the full sample of 51 systems, the concentration of poles toward the Galactic position  $l = 46.0^\circ$ ,  $b = 37^\circ$ , as observed in the 8.1 pc sphere, totally vanishes (the Rayleigh-Watson false-alarm probability then rises to 18%).

**Key words.** binaries: visual – binaries: spectroscopic – techniques: radial velocities – techniques: high angular resolution – methods: statistical – solar neighborhood

## 1. Introduction

In 1838, Mädler announced the probable existence of an astonishing phenomenon related to the orbital plane of visual double stars: they seem to be aligned with each other. This phenomenon has received quite some attention since then, but the most earliest studies that was based on data secured with old observational techniques and equipments, did not bring significant progress. In the years 1950–1967, Dommanget (with the assistance of Nys) re-investigated the question after collecting all available data needed to perform the first study based on a sample of orbits for which the orbital poles were determined unambiguously. This research (Dommanget 1968), updated in 1982–1987 (Dommanget 1988), confirmed Mädler's suspicion that the orbital poles of visual binaries in the solar neighbourhood do not seem to be oriented isotropically, but rather seem to cluster around the positions  $(l, b) \sim (100^\circ, -15^\circ)$  and  $(280^\circ, +15^\circ)$ . This claim was based on a limited number of objects (8 systems within 10 pc of the Sun and 70 systems

up to 25 pc), and was not subject to any analysis of its statistical significance. It was later confirmed by Glebocki (2000), who found that the poles of 19 systems within 10 pc of the Sun are concentrated around positions near  $(l, b) \sim (110^\circ, -10^\circ)$  and  $(-115^\circ, -5^\circ)$ , although the global distribution of 252 systems is isotropic. An historical overview of all these studies may be found in Dommanget (2014).

In this paper, we present the results of a new research conducted since 2005 within the framework of a collaboration between professional astronomers and amateur astronomers that are members of the Double Stars Committee of the Société Astronomique de France<sup>1</sup>.

Following the suggestion of Dommanget & Nys (2006), we re-investigated the question by concentrating on a very local data set. Moreover, to the best of our knowledge, it seems that the most recent list of orbital poles dates back to Batten (1967). Because the more recent studies did not publish the data sets on which they were based and because of the rapid increase of the number of available orbits, we feel the necessity to collect such data, and provide an updated list of orbital poles for binaries within 18 pc of the Sun.

\* Tables 1–3 and Appendices are available in electronic form at <http://www.aanda.org>

† Deceased October 1, 2014.

<sup>1</sup> <http://saf.etoiledoubles.free.fr/>

As already noted by [Finsen \(1933\)](#) and [Dommanget \(1968, 1988, 2005\)](#), a severe pitfall awaits the researcher on this topic: the ambiguity in the position of the ascending node, which, if not correctly assessed (Sect. 2), may ruin the distribution of the poles on the sphere.

To avoid this problem and establish a valid statistical material, we have first a) assembled a list of known visual binary orbits in the vicinity of the Sun for which a set of consistent and accurate radial-velocity measurements is available for solving the ambiguity of the orbital ascending node; and then b) computed the Galactic positions of the orbital poles of all systems for which the ambiguity of the orbital ascending node has been solved.

At first sight, some large-scale coherence in the process of binary formation might imply a non-random orientation of the poles on the celestial sphere. However, such a large-scale coherence is not expected to last after the coeval association has dissolved, since at any given time in the history of the Galaxy, stars in a given volume emanate from very different birth places and times, and their presence in a given volume is a momentary event. Therefore, given these potentially important (and problematic) consequences, any deviation from isotropy in the pole distribution should be firmly established before embarking on any physical discussion on the above questions.

In this new research, emphasis has been place on

- increasing the sample size with regard to previous studies;
- using dedicated tests to evaluate the statistical significance of any deviation from isotropy in the distribution of the orbital poles;
- analysing the evolution, as a function of the volume sampled, of such possible deviations from isotropy;
- discussing these results from the standpoint of Galactic kinematics.

This paper is structured as follows: in Sect. 2, we briefly recall the problem of unambiguously determining of the direction of the orbital pole, all mathematical details being provided in Appendix B. The master list of selected systems is presented in Sect. 3. For 51 systems up to 18 pc from the Sun, the distribution of the orbital poles on the sky is presented in Sect. 4. This section describes the available statistical tools used to analyse this distribution, and some indications about its degree of anisotropy are given. Possible selection effects in our sample is discussed in Sect. 5. The problem of possible orbital coplanarity in multiple systems is briefly discussed in Sect. 6. Section 7 discusses the question of the orientation of the orbital poles in the framework of Galactic kinematics. Conclusions and perspectives are given in Sect. 8. In Appendix A, notes are given on individual systems, along with new radial-velocity measurements used in the present study and, in several cases, new combined astrometric-spectroscopic orbits that resulted. In Appendix B, we recall the conventions adopted to define the relative orbit of a binary star, and we describe the method used to determine the ascending node and the direction of the orbital pole without any ambiguity.

## 2. Unambiguous determination of the orbital pole of a binary

The spatial orientation of the orbital planes of double stars is studied based on the knowledge of the orientation of their orbital poles.

It is well known that an essential problem in this type of study is that the orientation of the orbital pole is ambiguous for visual and astrometric binaries because two true orbits are compatible with the apparent orbit calculated from the astrometric observations: although the orbital inclination  $i$  is unambiguously determined, it is impossible to distinguish between the two possible values of the position angle  $\Omega$  of the ascending node. The problem can only be solved if radial-velocity measurements are available for at least one component of the system. Then, two scenarios may occur:

- i) for spectroscopic binaries resolved as visual or astrometric, the ascending node is immediately known unambiguously;
- ii) for visual or astrometry binaries for which radial-velocity measurements are available, the correct ascending node may be selected by comparing the trend of the measured radial velocities with the slope of the relative radial velocity curve computed from the orbit.

The conventions used in defining of the relative orbit of a binary as well as the details on the method used to solve the ambiguity of the ascending node and computing of the orientation of the orbital pole in Galactic coordinates are given in the Appendix B.

## 3. Data

The selection of the 95 systems in the master sample presented in Tables 1 and 2 was based on the availability of a visual or an astrometric orbit in the 6th Catalog of Orbit of Visual Binary Stars at USNO (6th COVBS<sup>2</sup>, [Hartkopf et al. 2001](#)) and of a HIPPARCOS parallax ([ESA 1997](#)) larger than 50 mas<sup>3</sup>. Table 1 lists various identifiers for the systems, such as their designations in the WDS (J2000 coordinates and the component designation taken in the 6th COVBS), CCDM, HIP or HIC, HD and SB9 (the 9th Catalogue of Spectroscopic Binary Orbits<sup>4</sup>), catalogs, and the discoverer name. Table 2 lists various physical data for the systems identified by their WDS designation (Col. 1). The parallax (Col. 2) is for all HIP entries from the revised HIPPARCOS Catalogue ([van Leeuwen 2007](#)), or from the paper listing the orbit otherwise. The spectral type (Col. 3) is generally taken from the Simbad database at the Centre de Données Astronomiques de Strasbourg (CDS; [Genova et al. 2000](#)). Columns 4 (orbital period), 5 (orbital semi-major axis), 6 (total mass of the system), 7 (mass ratio), 8 (Grade of the orbit) and 9 (reference of visual orbit) come from the 6th COVBS, or are directly derived from the catalogue data (the total mass of each system – Col. 6 – is computed from the orbital elements and the parallax using the third Kepler law), with the exception of the mass ratio (Col. 7), which is listed when available from SB2 or astrometry. Column 10 (“S.Orb”) lists either the reference of the spectroscopic orbit used to lift the ascending-node ambiguity, or “New” if the spectroscopic orbit has been computed in the present paper (see Appendix A), or “VD” if only the radial-velocity drift was used to lift the ambiguity, or “SD” if the sign of the velocity difference  $V_r(B) - V_r(A)$  was used to lift the ambiguity. Column 11, labelled “A”, contains a flag indicating whether the system has (or not) been considered in the final analysis: Y stands for yes,

<sup>2</sup> <http://ad.usno.navy.mil/wds/orb6.html>

<sup>3</sup> See also [Kirkpatrick et al. \(2012\)](#), who recently compiled an exhaustive list of stars nearer than 8 pc from the Sun, and [Raghavan et al. \(2010\)](#), who collected orbits for visual binaries with HIPPARCOS parallaxes larger than 40 mas and with primary spectral types F6-K3 (their Table 11).

<sup>4</sup> <http://sb9.astro.ulb.ac.be/intro.html>

NO stands for “no reliable visual orbit”, NV stands for “no radial velocities”, ND stands for “no visible drift in the velocities”, because either the period is too long or the velocities too inaccurate, and IC stands for inconclusive analysis. For systems with a combined visual and spectroscopic solution computed by [Pourbaix \(2000\)](#), the orbital elements were adopted without an additional verification because the method naturally lifts the ambiguity on the ascending node. The last column of [Table 2](#) identifies systems with an explanatory note (“n”) in [Appendix A](#) and triple or higher-multiplicity systems noted (“t”).

Radial-velocity measurements were searched for in the literature and among unpublished measurements obtained with the CORAVEL spectrovelocimeter ([Baranne et al. 1979](#)). A few more radial velocities were obtained especially for this purpose with the HERMES spectrograph installed on the *Mercator* 1.2 m telescope ([Raskin et al. 2011](#)). In the end, 51 systems from the master list comprising 95 binaries ([Table 2](#)) have radial velocities available that enable lifting the ambiguity on the ascending node. Hence the number of systems used in our analysis drops from 95 to 51, and the systems analysed all have  $d < 18$  pc.

For each system, the ambiguity on the ascending node was solved using one of the methods described in [Appendix B.3](#). The orbital pole orientation was been computed following the method of [Appendix B.4](#). In several cases, the radial velocities collected from the HERMES spectrograph ([Raskin et al. 2011](#)) or from the CORAVEL database ([Table A.1](#)) enable computing a new or updated spectroscopic binary orbit, as listed in [Tables A.2](#) and [A.3](#). These solutions were computed by combining the astrometric and spectroscopic data, following the method described by [Pourbaix \(2000\)](#). The orbital solutions are drawn in [Figs. A.2–A.8](#).

The positions of the orbital poles are listed in [Table 3](#). The column “Notes” identifies the entries for which a comment is provided in [Appendix A](#).

References to visual and spectroscopic orbits listed in [Table 2](#):

A1918b : [Aitken \(1918\)](#); Abt2006: [Abt & Willmarth \(2006\)](#); AST1999: [Franz et al. \(1999\)](#); AST2001: [Benedict et al. \(2001\)](#); B1960c: [van den Bos \(1960\)](#); Bag2005: [Balega et al. \(2005\)](#); Baz1980b: [Baize \(1980\)](#); Chg1972: [Chang \(1972\)](#); CIA2010: [Farrington et al. \(2010\)](#); Cou1960b: [Couteau \(1960\)](#); Doc1985c: [Docobo & Costa \(1985\)](#); Doc2008d: [Docobo et al. \(2008\)](#); Doc2010d: [Docobo & Ling \(2010\)](#); Dom1978: [Dommanget \(1978\)](#); Dru1995: [Drummond et al. \(1995\)](#); Duq1991b: [Duquenois et al. \(1991\)](#); Egg1956: [Eggen \(1956\)](#); Egn2008: [Eggenberger et al. \(2008\)](#); Fek1983: [Fekel & Tomkin \(1983\)](#); FMR2008b: [Rica Romero \(2008\)](#); Frv1999: [Forveille et al. \(1999\)](#); Gri1975: [Griffin & Emerson \(1975\)](#); Gri1998: [Griffin \(1998\)](#); Gri2004: [Griffin \(2004\)](#); Grr2000: [Girard et al. \(2000\)](#); Hal2002: [Han & Gatewood \(2002\)](#); Hei1974c: [Heintz \(1974\)](#); Hei1984a: [Heintz \(1984\)](#); Hei1986: [Heintz \(1986\)](#); Hei1987b: [Heintz \(1987\)](#); Hei1988d: [Heintz \(1988\)](#); Hei1990c: [Heintz \(1990a\)](#); Hei1990d: [Heintz \(1990b\)](#); Hei1994a: [Heintz \(1994\)](#); Hei1994b: [Heintz & Cantor \(1994\)](#); Hei1996: [Heintz \(1996\)](#); HIP1997d: [ESA \(1997\)](#); Hle1994: [Hale \(1994\)](#); Hnk2011: [Hinkley et al. \(2011\)](#); Hop1958: [Hopmann \(1958\)](#); Hop1973a: [Hopmann \(1973\)](#); Hrt1996a: [Hartkopf et al. \(1996\)](#); Hrt2003: [Hartkopf & Mason \(2003\)](#); Irw1996: [Irwin et al. \(1996\)](#); Jnc2005: [Jancart et al. \(2005\)](#); Kam1989: [Kamper et al. \(1989\)](#); Kiy2001: [Kiyaveva et al. \(2001\)](#); Knc2010: [Konacki et al. \(2010\)](#); Lip1967: [Lippincott \(1967\)](#); Lip1972: [Lippincott \(1972\)](#); Llo2007: [Martinache et al. \(2007\)](#); Maz2001: [Mazeh et al. \(2001\)](#); Mnt2000a: [Mante \(2000\)](#); Msn1995: [Mason et al. \(1995\)](#); Msn1999a: [Mason et al. \(1999\)](#); Msn2011c: [Mason & Hartkopf \(2011\)](#); Mut2010b: [Muterspaugh et al. \(2010a\)](#); Mut2010c: [Muterspaugh et al. \(2010b\)](#); Nid2002: [Nidever et al. \(2002\)](#); Pbx2000b: [Pourbaix \(2000\)](#); Pbx2002:

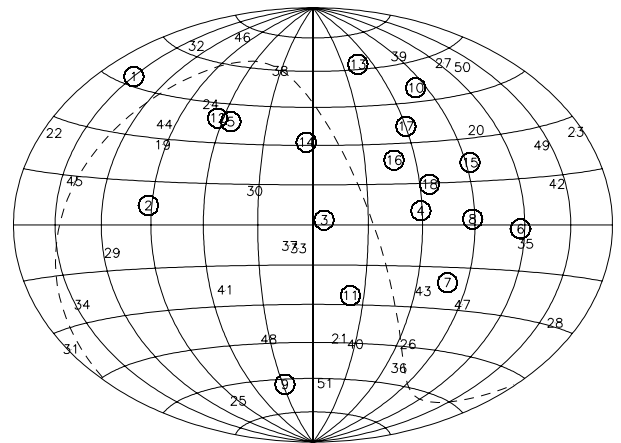


**Fig. 1.** Positions of the orbital poles on the sky, with the grid representing Galactic coordinates. The Galactic centre is at the centre of the grid. The systems are labelled by their numbers of [Table 3](#). The circled labels identify the systems up to  $N = 18$  whose distribution is the most significantly different from isotropic according to [Fig. 3](#). The dashed line displays the celestial equator. For comparison, the ecliptic pole is located at  $l = 96.4^\circ, b = 30^\circ$ .

[Pourbaix et al. \(2002\)](#); PkO2006b: [Gorshanov et al. \(2006\)](#); Pop1996b: [Popovic & Pavlovic \(1996\)](#); Sca2002c: [Scardia \(2002\)](#); Sca2007c: [Scardia et al. \(2007\)](#); Sgr2000: [Ségransan et al. \(2000\)](#); Sgr2012: [Barry et al. \(2012\)](#); Sod1999: [Söderhjelm \(1999\)](#); Str1969a: [Strand \(1969\)](#); Str1977: [Strand \(1977\)](#); USN1988a: [Dahn et al. \(1988\)](#); USN1988b: [Geyer et al. \(1988\)](#); USN2002: [Seymour et al. \(2002\)](#); vAb1957: [van Albada \(1957\)](#); Wie1957: [Wieth-Knudsen \(1957\)](#); Zir2003: [Zirm \(2003\)](#); Zir2011: [Zirm \(2011\)](#).

## 4. Distribution of the orbital poles on the sky

[Figure 1](#) displays the distribution on the sky in galactic coordinates of the orbital poles listed in [Table 3](#), for systems up to 18 pc. After estimating in [Sect. 4.1](#) the typical errors affecting the orbital-pole positions, we describe in [Sect. 4.2](#) the available statistical tools for studying the possible deviation from isotropy of the distribution of orbital poles on the sky.

### 4.1. Estimating the error on the orbital-pole positions

To evaluate the typical error affecting the orbital-pole positions, we used a Monte Carlo approach because of the complexity of the algebraic relations that link the orbital elements and the system position to the orbital-pole position (Eqs. (B.4) to (B.7)). We used the system WDS 00057+4549 (HD 38) as a test case because it is one of the systems with the longest-period for which we lifted the ascending-node ambiguity. Even though the error on the orbital period is large ( $P = 509.6 \pm 100.0$  yr), only the uncertainties on the inclination  $i$  and on the longitude of the ascending node  $\Omega$  affect the uncertainty on the pole position. For WDS 00057+4549, we therefore adopted:  $\alpha = 1.4209^\circ$ ,  $\delta = 45.81^\circ$ ,  $i = 54.9^\circ \pm 2.4^\circ$ , and  $\Omega = 13.5^\circ \pm 2.3^\circ$ , according to the orbit computed by [Kiyaveva et al. \(2001\)](#). We drew  $10^4$  ( $i, \Omega$ ) pairs from this average and standard-deviation values, assuming that they follow a normal distribution; we then derived the orbital pole position for each of these cases from Eqs. (B.4) to (B.7). The results are displayed in [Fig. 2](#). The Gaussian fits to the resulting longitude and latitude distributions (bottom panel), show – as expected – that the uncertainties on  $i$  and  $\Omega$  directly propagate onto the polar position ( $2.3^\circ$  and  $2.0^\circ$  in Galactic

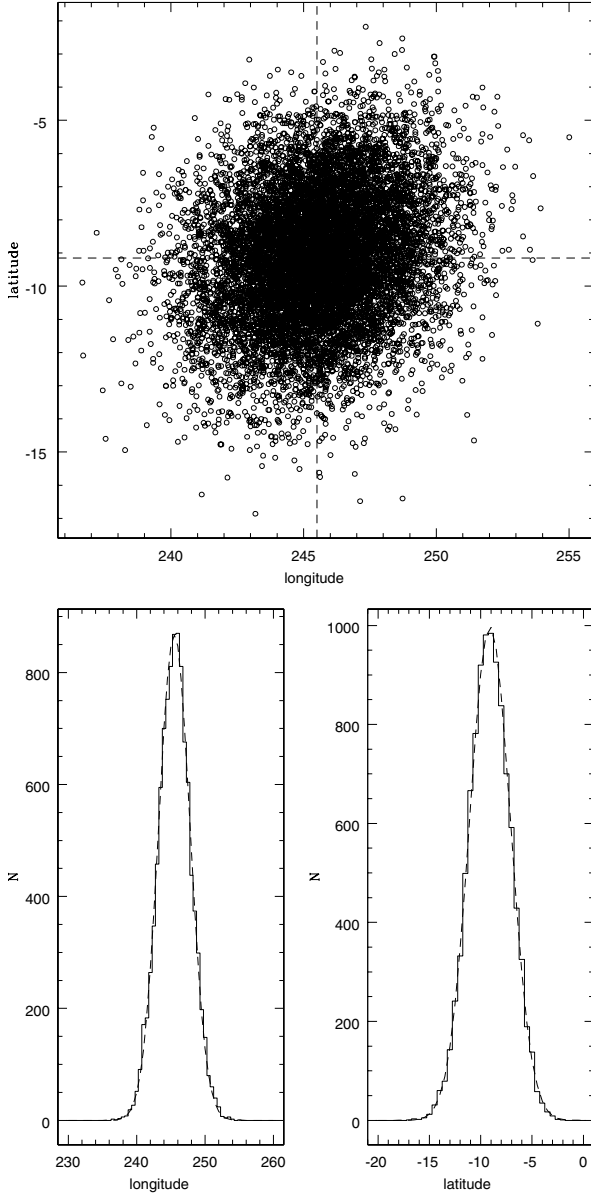


**Fig. 2.** *Top panel:* distribution of the orbital-pole positions on the sky, drawn from the normal distributions for  $i = 54.9^\circ \pm 2.4^\circ$  and  $\Omega = 13.5^\circ \pm 2.3^\circ$  corresponding to the benchmark system WDS 00057+4549. The intersection of the dashed lines marks the nominal pole position. As expected, the distribution is centred on this nominal position. *Bottom panel:* histograms corresponding to the longitude and latitude distributions. The dashed lines correspond to Gaussian distributions centred on the nominal pole position, with standard deviations of  $2.3^\circ$  and  $2.0^\circ$  in Galactic longitude and latitude, respectively.

longitude and latitude, respectively, for WDS 00057+4549). If the uncertainties on  $i$  and  $\Omega$  are unequal, the resulting distribution of the orbital poles will simply be tilted with respect to the axis frame. In the analysis of the pole distribution presented below, one should therefore keep in mind that these positions are subject to an uncertainty of the same order as that on  $i$  and  $\Omega$ .

#### 4.2. Available statistical tools

The current section is mainly based on Gillett (1988), Upton & Fingleton (1989), and Briggs (1993). In this section, we discuss how to test the null hypothesis that the pole distribution is

isotropic. The simplest test is the Rayleigh test (Fisher 1953; Briggs 1993). For the purpose of Rayleigh statistics, the  $i = 1, \dots, N$  poles are represented by unit vectors  $(x_i, y_i, z_i)$  (with  $x_i^2 + y_i^2 + z_i^2 = 1$ ), and one computes

$$\mathcal{R}^2 = (\sum_{i=1}^N x_i)^2 + (\sum_{i=1}^N y_i)^2 + (\sum_{i=1}^N z_i)^2, \quad (1)$$

where  $\mathcal{R}$  representing the module of the vectorial sum of the  $N$  unit vectors  $(x_i, y_i, z_i)$ . This vectorial sum gives the orientation of the dipole of the distribution. If the poles are isotropically distributed, the unit vectors representing their orientation will tend to cancel each other out and the resulting  $\mathcal{R}$  will be close to zero, while if the poles have a preferential orientation,  $\mathcal{R}$  will tend to be larger than expected for the isotropic distribution. However, there could be very specific anisotropic situations leading to low  $\mathcal{R}$  values, for instance one with an even number of poles distributed in a bimodal distribution with the modes aligned in exactly opposite directions, and equal numbers of poles populating both modes. This underlines the fact that a test such as the Rayleigh test should always be carried out against an alternative model, and this model must be chosen on physical grounds (Gillett 1988). The most natural alternative to be used with Rayleigh's test is the Fisher distribution (Fisher 1953; Watson 1956), which is unimodal and assumes symmetry about the mean. Obviously, this bimodal situation does not follow a Fisher distribution, and Rayleigh's test has therefore no power to distinguish it from isotropy (i.e., the second-kind risk of accepting the null hypothesis of isotropy while it is false is high). The combined statistic of Giné (1975), which are described below (Eq. (17)), is the most powerful against all alternatives (Gillett 1988).

The Rayleigh statistics may be used as a test of isotropy against a unimodal distribution by calculating the probability  $\alpha_{\mathcal{R}}$  of obtaining a value of  $\mathcal{R}$  greater than or equal to the observed value  $\mathcal{R}_{\text{obs}}$  assuming that the data are drawn from the isotropic distribution (Watson 1956, 1983):

$$\alpha_{\mathcal{R}} = P(\mathcal{R} \geq \mathcal{R}_{\text{obs}}) = \int_{\mathcal{R}_{\text{obs}}}^N f_{\mathcal{R}}(R) dR, \quad (2)$$

where  $f_{\mathcal{R}}$  is the probability density function for  $\mathcal{R}$  (i.e., the probability of finding  $\mathcal{R}$  between  $R$  and  $R + dR$  is  $f_{\mathcal{R}}dR$ ). Its detailed expression may be found in Fisher (1953) and Briggs (1993). If  $\alpha_{\mathcal{R}}$  is small, then the poles are very unlikely to have been drawn from an isotropic parent population. Under such circumstances, it is said that the observed pole distribution is inconsistent with isotropy at the  $1 - \alpha_{\mathcal{R}}$  confidence level. It means that there is a (first-kind) risk  $\alpha_{\mathcal{R}}$  of rejecting the null hypothesis of isotropy while it is actually true. Stephens (1964) provides a table of critical values for  $\mathcal{R}$  for  $\alpha_{\mathcal{R}} = 1, 2, 5$  and 10%.

While the Rayleigh statistics is valid for any value of  $N$ , there exists a more convenient form of it at large  $N$  ( $\geq 50$ ), known as the Rayleigh-Watson statistics  $\mathcal{W}$  (Watson 1956, 1983):

$$\mathcal{W} = \frac{3}{N} \mathcal{R}^2. \quad (3)$$

Upton & Fingleton (1989) used the table of Stephens (1964) to devise an improved approximation, which works well even for low values of  $N$ :

$$\mathcal{W}^* = \frac{3}{N - c(\alpha)} \mathcal{R}^2. \quad (4)$$

$\mathcal{W}^*$  follows a  $\chi^2$  distribution with three degrees of freedom. For convenience, the values of the correction factor  $c(\alpha)$  for the

**Table 4.** Values of the correction factor  $c(\alpha)$  for the Rayleigh test, from Upton & Fingleton (1989).

Significance level $\alpha$	10%	5%	1%
$c(\alpha)$	0.121	0.278	0.630
Reference value $\chi_3^2(\alpha)$	6.25	7.81	11.34

Rayleigh test are reproduced from Upton & Fingleton (1989) in Table 4. A value  $\mathcal{W}^* > 11.34$  indicates that there is a significant concentration of poles toward one direction (with a confidence level of 99%).

Instead of considering  $\mathcal{R}$  as the length of the resulting dipole vector, it may be useful to consider it as the distance from the origin achieved by a random walk of  $N$  unit steps. A well-known result from the random-walk theory then states that  $\langle \mathcal{R}^2 \rangle = N$ , from which it follows that  $\langle \mathcal{W} \rangle = 3$ . It is therefore not surprising that the statistic  $\mathcal{W}$  is asymptotically distributed as a  $\chi^2$  distribution with three degrees of freedom (Watson 1956, 1983), so that

$$\alpha_{\mathcal{W}^*} = P(\mathcal{W}^* \geq \mathcal{W}_{\text{obs}}^*) = \int_{\mathcal{W}_{\text{obs}}^*}^{\infty} f_{\chi_3^2}(x) dx = F_{\chi_3^2}(\mathcal{W}^* \geq \mathcal{W}_{\text{obs}}^*), \quad (5)$$

where  $f_{\chi_3^2}$  is the probability density of  $\chi_3^2$  and  $F_{\chi_3^2}$  is the upper cumulative probability distribution function of  $\chi_3^2$ . Obviously, the latter function is much easier to evaluate than the corresponding one for the Rayleigh statistics (Eq. (2)). An additional advantage of this statistics is that it is asymptotically independent from  $N$ .

Again, the isotropy of the data may be tested by calculating the observed statistics  $\mathcal{W}_{\text{obs}}^*$  and the corresponding probability  $\alpha_{\mathcal{W}}$ , which has a similar interpretation as the one given above for  $\alpha_{\mathcal{R}}$ . For large  $N$ ,  $\alpha_{\mathcal{R}} = \alpha_{\mathcal{W}}$ , and the two tests are equivalent.

We stress here an important result from the hypothesis-testing theory: although the *first-kind risk* (of rejecting the null hypothesis of isotropy while it is true, also known as the false-alarm probability) is controlled by the adopted confidence level  $1 - \alpha_{\mathcal{R}}$ , the *second-kind risk* (of accepting the null hypothesis of isotropy while it is false, also known as the power of the test) is not controlled as easily, since this second-kind risk depends on the exact nature of the true underlying distribution. This was well illustrated above with the Rayleigh test which is said to have no power against a bimodal distribution. Because different statistical tests have different powers it is important not to use only one if one does not know the actual underlying distribution.

Since the Rayleigh test is not appropriate when the alternative is a bimodal axial distribution, for testing uniformity when the alternative is such, we must turn to tests based upon the properties of statistics involving the eigenvalues of the quadrupolar matrix  $\mathbf{M}_N$  (Watson 1966, 1983; Briggs 1993):

$$\mathbf{M}_N = \frac{1}{N} \sum_{i=1}^N \begin{bmatrix} x_i x_i & x_i y_i & x_i z_i \\ y_i x_i & y_i y_i & y_i z_i \\ z_i x_i & z_i y_i & z_i z_i \end{bmatrix}. \quad (6)$$

Since  $\mathbf{M}_N$  is real and symmetric, it has three eigenvalues  $\lambda_k$ , and since it has unit trace, the sum of its eigenvalues  $\lambda_k$  is one<sup>5</sup>. Moreover, the diagonal elements are sums of squares. In the coordinate system in which  $\mathbf{M}_N$  is diagonal, the diagonal elements are the eigenvalues, and therefore the eigenvalues are not negative. If the poles were drawn from the isotropic distribution,

then, excepting statistical fluctuations, the eigenvalues  $\lambda_k$  should be equal, and since  $\mathbf{M}_N$  has unit trace,  $\lambda_k = 1/3$ .

If the alternative to isotropy is a *rotationally asymmetric* axial distribution<sup>6</sup>, the Bingham statistics  $\mathcal{B}$  is appropriate: it measures the deviation of the eigenvalues  $\lambda_k$  of the quadrupolar matrix  $\mathbf{M}_N$  from the value  $1/3$  expected for isotropy (Bingham 1974; Watson 1983):

$$\mathcal{B} = \frac{15N}{2} \sum_{k=1}^3 \left( \lambda_k - \frac{1}{3} \right)^2. \quad (7)$$

The statistics  $\mathcal{B}$  is asymptotically distributed as a  $\chi^2$  distribution with five degrees of freedom, so that

$$\alpha_{\mathcal{B}} = P(\mathcal{B} \geq \mathcal{B}_{\text{obs}}) = \int_{\mathcal{B}_{\text{obs}}}^{\infty} f_{\chi_5^2}(x) dx = F_{\chi_5^2}(\mathcal{B} \geq \mathcal{B}_{\text{obs}}), \quad (8)$$

where  $f_{\chi_5^2}$  is the probability density function of  $\chi_5^2$  and  $F_{\chi_5^2}$  is the upper cumulative probability distribution function of  $\chi_5^2$ . Again, if  $\alpha_{\mathcal{B}}$  is very small, the hypothesis of isotropy is contradicted and rejected with a first-kind risk of  $\alpha_{\mathcal{B}}$ . Briggs (1993) showed that  $\alpha_{\mathcal{B}}$  as derived from Eq. (8) overestimates the true first-kind risk when  $N < 20$  for  $\alpha_{\mathcal{B}} = 0.05$ , and when  $N < 40$  for  $\alpha_{\mathcal{B}} = 0.01$ . In other words, under these circumstances,  $1 - \alpha_{\mathcal{B}}$  will underestimate the statistical confidence with which the hypothesis of isotropy can be rejected.

If the alternative to isotropy is a *rotationally symmetric* axial distribution (either a bipolar distribution along a given direction, or a girdle with rotational symmetry, both known as the Dimroth-Watson distribution; Upton & Fingleton 1989), the Bingham test is still applicable, but two of the three eigenvalues will then be close to each other (Bingham 1974, and below). Assuming that the pole of the distribution is located at  $\phi_0 = 0^\circ$  and  $\theta_0 = 0^\circ$  ( $(\phi, \theta)$  being a polar coordinate system on the sphere, with  $\phi$  the azimuthal angle, and  $\theta$  the polar angle), Mardia & Jupp (2000) showed that  $(\hat{\phi}_0, \hat{\theta}_0)$ , the maximum likelihood estimate of the polar direction, is related to the eigenvectors of the  $\mathbf{M}_N$  matrix; a girdle distribution will have its symmetry axis along  $\mathbf{e}_1$ :

$$\mathbf{e}_1 = (\sin \hat{\theta}_0 \cos \hat{\phi}_0, \sin \hat{\theta}_0 \sin \hat{\phi}_0, \cos \hat{\theta}_0) \quad \text{and} \quad \lambda_1 < \lambda_2 \sim \lambda_3, \quad (9)$$

whereas an axial distribution will have  $\mathbf{e}_3$  as symmetry axis<sup>7</sup>:

$$\mathbf{e}_3 = (\sin \hat{\theta}_0 \cos \hat{\phi}_0, \sin \hat{\theta}_0 \sin \hat{\phi}_0, \cos \hat{\theta}_0) \quad \text{and} \quad \lambda_1 \sim \lambda_2 < \lambda_3. \quad (10)$$

In the general case of a *rotationally asymmetric* axial distribution, one has  $\lambda_2 - \lambda_1$  and  $\lambda_3 - \lambda_1$  large and non-equal (girdle), or  $\lambda_3 - \lambda_1$  and  $\lambda_3 - \lambda_2$  large and non-equal (polar).

Anderson & Stephens (1972) showed that  $\lambda_1$  and  $\lambda_3$  themselves are the most appropriate test statistics for the comparison of the hypothesis of uniformity against that of a Dimroth-Watson distribution. Upton & Fingleton (1989) have used the tables computed by Anderson & Stephens (1972) to devise critical values of  $\lambda_1$  and  $\lambda_3$  at confidence level  $\alpha$ . A significant departure from isotropy towards the girdle form of the Dimroth-Watson distribution is judged to have occurred if  $\lambda_1 < \lambda_1(\alpha)$ , where

$$\lambda_1(\alpha) = \frac{1}{3} + \frac{a_1(\alpha)}{\sqrt{N}} + \frac{b_1(\alpha)}{N} + \frac{c_1(\alpha)}{N\sqrt{N}}, \quad (11)$$

<sup>6</sup> In other words, the data points are non-uniformly distributed along a ring.

<sup>7</sup> We recall that the eigenvalues are ordered so that  $\lambda_3 \geq \lambda_2 \geq \lambda_1$ .

<sup>5</sup> The eigenvalues are ordered so that  $\lambda_3 \geq \lambda_2 \geq \lambda_1$ .

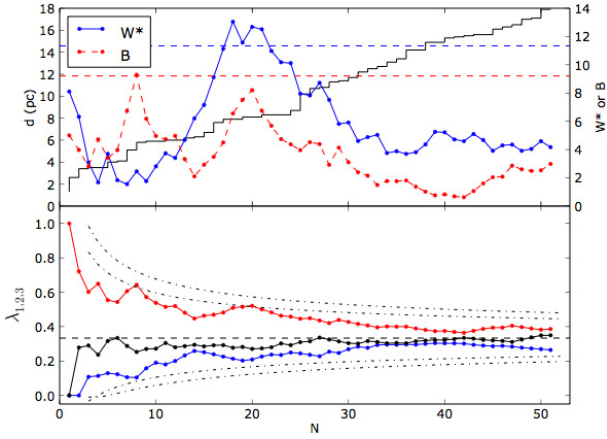


**Fig. 3.** Upper panel: evolution of the Rayleigh-Watson  $\mathcal{W}^*$  (blue dashed line, and right-hand scale; the correction to  $\mathcal{W}$  – Eq. (4) – has been made for a confidence level  $\alpha$  of 1%) and Bingham  $\mathcal{B}$  (red dot-dashed line, and right-hand scale) statistics as a function of the number of systems. The horizontal blue dashed curve corresponds to a first-kind risk of 1% of rejecting the null hypothesis of isotropy while it is true, based on the  $\mathcal{W}^*$  statistics. The horizontal red dashed line is the 10% first-kind risk for the  $\mathcal{B}$  statistics. The number of systems as a function of distance is given by the black solid line and left-hand scale. Isotropy corresponds to  $\mathcal{B} \rightarrow 0$  and  $\mathcal{W} \rightarrow 3$ . Lower panel: three eigenvalues of the orientation matrix (Eq. (6)). Isotropy corresponds to  $\lambda_{1,2,3} = 1/3$ , as seen at large distances. The critical values for  $\lambda_{1,3}$  corresponding to  $\alpha = 1\%$  and  $10\%$  as given by Eqs. (11) and (12) are displayed by the dash-dotted lines.

whereas a significant departure towards the bipolar form of the distribution is judged to have occurred if  $\lambda_3 > \lambda_3(\alpha)$ , where

$$\lambda_3(\alpha) = \frac{1}{3} + \frac{a_3(\alpha)}{\sqrt{N}} + \frac{b_3(\alpha)}{N}, \quad (12)$$

where the coefficients  $a_{1,3}(\alpha)$ ,  $b_{1,3}(\alpha)$ , and  $c_1(\alpha)$  have values that depend on the significance level,  $\alpha$ . These values may be found in Table 10.15 of Upton & Fingleton (1989). The values  $\lambda_1(\alpha)$  and  $\lambda_3(\alpha)$  have been plotted as dashed lines in the lower panel of Fig. 3 for  $\alpha = 1\%$  and  $10\%$ .

In summary, by combining the Rayleigh-Watson statistics with the Bingham statistic, the isotropy of the distribution may be distinguished among several alternatives, since a value  $\mathcal{W} > 3$  reveals that there is a concentration of poles toward one direction, but values close to 3 indicate that the distribution is either isotropic or bipolar. The bipolarity of the distribution is in turn assessed from  $\lambda_3 > \lambda_3(\alpha)$ . To summarize (see also Table 1 of Briggs 1993; and Table 10.7 of Upton & Fingleton 1989):

- unipolar distribution around one end of the eigenvector  $\mathbf{e}_3$ :

$$\mathcal{W} > 3: \quad \lambda_{1,2} < 1/3 < \lambda_3, \quad (13)$$

- bipolar distribution around both ends of the eigenvector  $\mathbf{e}_3$ :

$$\mathcal{W} \sim 3: \quad \lambda_{1,2} < 1/3 < \lambda_3, \quad (14)$$

- girdle orthogonal to the eigenvector  $\mathbf{e}_1$ :

$$\mathcal{W} \sim 3: \quad \lambda_1 < 1/3 < \lambda_{2,3}. \quad (15)$$

Finally, one should mention the non-parametric statistical tests that do not presuppose any alternative model. They are thus more general than tests against a specific alternative, but for

that reason are also less powerful (i.e., have a higher risk of accepting the null hypothesis of isotropy while it is false; Gillett 1988; Mardia & Jupp 2000). To test against alternatives that are asymmetric with respect to the centre of the sphere, Beran’s  $B$  test (Beran 1968) is the most powerful:

$$B = N - \frac{4}{N\pi} \sum_{i < j}^N \Psi_{ij} = N - \frac{2}{N\pi} \sum_i^N \sum_j^N \Psi_{ij}. \quad (16)$$

To test against symmetric or axial alternatives, Giné’s test  $G$  (Giné 1975) is the most powerful:

$$G = \frac{N}{2} - \frac{4}{N\pi} \sum_{i < j}^N \sin \Psi_{ij} = \frac{N}{2} - \frac{2}{N\pi} \sum_i^N \sum_j^N \sin \Psi_{ij}. \quad (17)$$

The combined Giné statistic  $F = B + G$  tests against all alternatives. In Eqs. (16) and (17),  $N$  is the number of data points, and  $\Psi_{ij} = \cos^{-1}(\mathbf{x}_i \cdot \mathbf{x}_j)$  is the smaller of the angles between poles  $\mathbf{x}_i$  and  $\mathbf{x}_j$ . High values of these statistics suggest departure from isotropy. Critical values for various percentage levels of significance for  $B$ ,  $G$  and  $F$  have been calculated by Keilson et al. (1983). In the large-sample limiting distribution of  $F$ , the 10%, 5%, and 1% confidence levels are 2.355, 2.748, and 3.633, respectively.

#### 4.3. Isotropic or anisotropic?

In this section, we apply the methods outlined in Sect. 4.2 to the sample of orbital poles listed in Table 3. The top panel of Fig. 3 displays the evolution of the Rayleigh-Watson  $\mathcal{W}^*$  and Bingham  $\mathcal{B}$  statistics as a function of distance, thus for an increasing number of systems.

The various statistical indicators described in Sect. 4.2 are listed in Table 5 separately for the 20 systems up to 8.1 pc, and for all 51 systems closer than 18 pc. For estimating  $\alpha_{\mathcal{W}^*}$  and  $\alpha_{\mathcal{B}}$ , the asymptotically equivalent  $\chi_3^2$  and  $\chi_5^2$  distributions were used, respectively.

For the 20 systems with  $d \leq 8.1$  pc, the Rayleigh-Watson test  $\mathcal{W}^*$  signals a very significant deviation from isotropy<sup>8</sup>, with a (first-kind) risk of  $\alpha_{\mathcal{W}^*} = 0.5\%$  of rejecting the null hypothesis of isotropy while it is actually true (Table 5). The Beran test (for isotropy against alternatives that are asymmetric with respect to the centre of the sphere) provides an identically significant result ( $B = 3.32$  or  $\alpha \sim 0.7\%$ ; Keilson et al. 1983).

As seen from Table 5, the Bingham and Giné tests are less conclusive, but this is easily understood. The Giné test, being “universal” (it tests against all alternatives), is less efficient than Rayleigh-Watson’s in the sense that it requires a stronger deviation from isotropy to yield similarly low  $\alpha$  values. Bingham test being devised against symmetric alternatives, which is not the situation encountered in our data (Fig. 1), it is not efficient either in the situation under study, and should not be given much consideration.

Another way to understand why the Rayleigh-Watson and Bingham statistics yield vastly different significance levels is remembering that the Rayleigh-Watson and Bingham statistics test for the presence of a dipole or of a quadrupole, respectively, in the distribution of poles on the sphere (Hartmann & Epstein 1989; Briggs 1993, and Sect. 4.2). As already discussed in relation with Eq. (1), the vector  $\mathcal{R}$  is the dipole moment of the distribution, whereas the eigenvectors of the quadrupole matrix  $\mathbf{M}_N$

<sup>8</sup> As apparent from Fig. 3, restricting the sample to 18 systems would yield an even more significant result, but this would imply considering only one orbital pair from the triple system WDS 11182+3132 (Table 3), which is not physically sound. A discussion of the problem of triple systems is presented in Sect. 6.

**Table 5.** Various isotropy indicators, listed separately for the 20 systems up to 8.1 pc, and for all 51 systems up to 18 pc.

$N$	$\bar{x}$	$\bar{y}$	$\bar{z}$	$\mathcal{R}$	$\mathcal{W}$	$\mathcal{W}^*$	$\alpha_{\mathcal{W}}$	$\lambda_3$	$\lambda_2$	$\lambda_1$	$\mathcal{B}$	$\alpha_{\mathcal{B}}$	$B$	$\alpha_B$	$G$	$\alpha_G$
Systems closer than 8.1 pc																
20	0.254	0.262	0.268	9.05	12.28	12.68	0.005	0.52	0.27	0.21	8.20	0.14	3.32	0.007	0.65	0.19
All systems up to 18 pc																
51	0.071	0.109	0.100	8.36	4.11	4.17	0.18	0.39	0.35	0.26	2.98	0.70	1.22	0.20	0.32	0.80

**Notes.** See Sect. 4.2 for the definition of the various indicators.  $\bar{x}$ ,  $\bar{y}$  and  $\bar{z}$  are the average of  $(x_i, y_i, z_i)$ . The Watson statistics has first been corrected by Eq. (4) for  $\alpha = 1\%$ , before being approximated by the  $\chi^2_3$  statistic so as to compute  $\alpha_{\mathcal{W}^*}$ . The columns labelled  $B$  and  $G$  refer to Beran and Giné statistics, respectively (Eqs. (16) and (17)).

are related to the orientation of the quadrupolar component of the distribution (see the discussion in relation with Eqs. (13)–(15)). Therefore, the dipolar vector and the eigenvector  $e_3$  associated with the highest eigenvalue of  $\mathbf{M}_N$  ought to be different. For the considered orbital-pole distribution, the largest dipole moment is obtained for the  $N = 20$  closest systems and points in the direction  $l = 46.0^\circ$ ,  $b = 36.7^\circ$ , with a clear deficit of poles in the opposite direction. On the other hand, the eigenvector  $e_3$  associated with the highest eigenvalue  $\lambda_3 = 0.52$  for  $N = 20$  points towards  $l = 77.4^\circ$ ,  $b = 8.4^\circ$ . These directions are similar, albeit not identical, and obviously point in the direction of a higher concentration of poles (Fig. 1).

The Rayleigh-Watson (dipolar) test yields a deviation from isotropy that is more significant than the Bingham (quadrupolar) test. Figure 3 indeed signals that the eigenvalues  $\lambda_{1,2,3}$  and  $\mathcal{W}^*$  fulfill Eq. (13) that corresponds to a unipolar distribution.

To evaluate the robustness of the low first-kind risk obtained for the Rayleigh-Watson statistics, a jackknife approach was used, that is, we repeated the above procedure of computing  $\mathcal{W}^*$  as a function of distance (or sample size, with systems ordered by increasing distance from the Sun) after removing one system at a time from the full sample. Since  $\mathcal{W}^*$  peaks around  $N = 20$ , it was sufficient to do so for the 25 systems closest to the Sun, removing one system at a time. This way, 25 curves of  $\mathcal{W}^*$  as a function of  $N$  were generated, one for each of the 25 samples thus generated. These curves are presented in Fig. 4 and are similar to the curve presented in the upper panel of Fig. 3. The thick line in Fig. 4 corresponds to all systems being considered (thus identical to the curve in the upper panel of Fig. 3). The lower (red) line is the one corresponding to the sample with system No. 16 removed (since this system is the one weighting heavily in the original  $\mathcal{W}^*$  peak; the number refers to Table 3 and Fig. 1). As expected, this curve has the lowest significance, peaking at only 1.5% instead of 0.5% in the full sample. The other thin curves are for all the other samples, as explained above. Figure 4 thus provides a fair evaluation of the robustness of the alarm signal: indeed, after removing system No. 16, the false-alarm probability just misses 1% and is thus not especially significant; but removing closer systems (such as Nos. 1 or 2, i.e., systems far away from the pole cluster seen in Fig. 1) makes the curve rocket to 0.1% significance! In summary, the fluctuations caused by the small sample size causes the highest  $\mathcal{W}^*$  significance level to vary between 1.5 and 0.1%! The reality of the deviation from isotropy can thus not be assessed with certainty at this stage, given the small number of systems available, and despite our efforts to increase it.

The fact that this deviation from isotropy does not appear for subsamples with cutoff distances shorter than 8 pc moreover decreases its *physical* significance. One could have envisioned for instance a situation where the  $\mathcal{W}^*$  index maintains statistically significant values all the way to 8 pc, and then fades to insignificant values at larger distances. But the first part of that

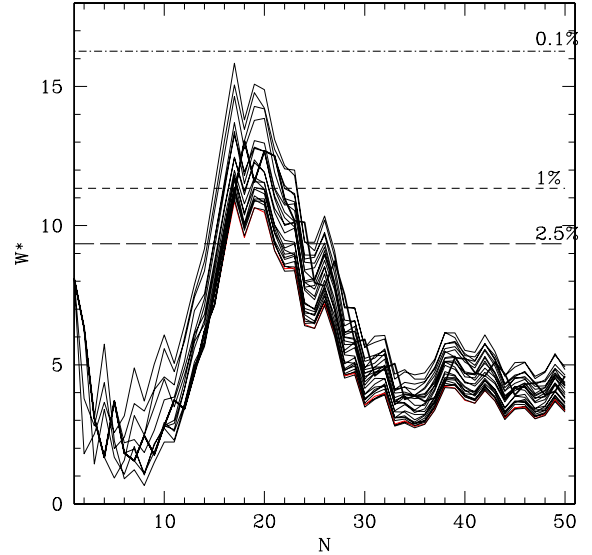


**Fig. 4.** Evolution of the Rayleigh-Watson  $\mathcal{W}^*$  statistics as a function of the number of systems in a jackknife approach. Each curve thus corresponds to the full sample with one system removed. The thick line corresponds to the full sample (same as the blue dashed line in the upper panel of Fig. 3). The lowest thin (red) line corresponds to the sample with system No. 16 removed (WDS 14514+1906). False-alarm probabilities of 2.5, 1, and 0.1% are depicted by the dashed horizontal lines.

statement is not fulfilled: the closest 15 systems (up to 6 pc) have  $\alpha(\mathcal{W}^*) > 5\%$  (Fig. 3). At distances larger than 8 pc, the significance of the deviation from isotropy fades away again, at least for the Bingham statistics:  $\mathcal{B} \rightarrow 0$ ,  $\lambda_{1,2,3} \rightarrow 1/3$ . The rise of  $\mathcal{B}$  above 2.5 for  $N > 47$  is not at all significant since it corresponds to  $\alpha_{\mathcal{B}} = 0.79$ . In contrast, the Rayleigh-Watson statistics  $\mathcal{W}^*$  does not drop to its isotropic value of 3, but rather stays around 4, corresponding to a first-risk probability of about 18% of rejecting the null hypothesis of isotropy despite being true. Indeed, the addition of systems farther away than 8 pc does not fully destroy the anisotropy that appeared in the 8 pc sphere, since a deficit of poles remain around  $l = 270^\circ$ ,  $b = -30^\circ$  (Fig. 1).

We thus conclude that the poles of the binary systems within 8 pc of the Sun exhibit a weak tendency to cluster around  $l = 46^\circ$ ,  $b = 37^\circ$  (which, incidentally, is not far from the pole of the ecliptic). The systems numbered 15–18 and 20 (see Table 3) are responsible for that clustering, which fades away if shorter or larger sampling distances are considered.

## 5. Impact of selection effects

As Blaauw appropriately commented after Batten’s talk on the topic of the present paper during the IAU symposium 30 (Batten 1967), the possibility that observational selection effects could

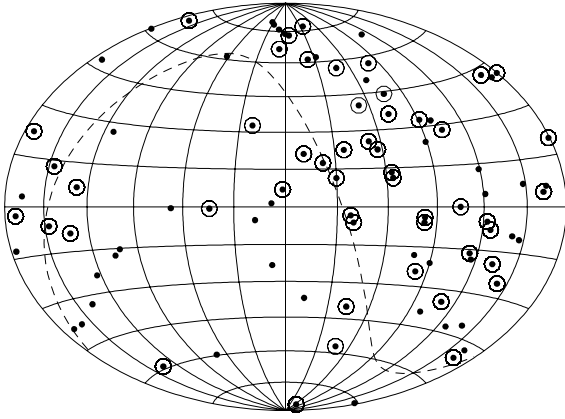


**Fig. 5.** Location of binary systems from Table 2 in Galactic coordinates, with the galactic centre in the middle of the map. The circles identify the systems with an unambiguously defined pole, as plotted in Fig. 1. The dashed line is the celestial equator.

actually be causing an anisotropy in the pole distribution should be considered. Figure 5 indeed reveals that the studied systems are concentrated in the northern equatorial hemisphere, since lifting the pole ambiguity requires radial velocities that are easier to obtain for northern hemisphere targets (combined with the fact that the astronomy of visual double stars relies on a longer time-base in the northern hemisphere; hence long periods are more commonly derived for northern targets). Could this anisotropic initial distribution be the cause for the pole anisotropy observed in the 8 pc sphere around the Sun?

For this to be the case, there should be a correlation between the position of the binary on the sky and the position of its orbital pole. A non-uniform celestial distribution of the systems studied (as observed in Fig. 5) would then propagate onto their orbital-pole distribution. A correlation between system position and pole position would manifest itself as a non-uniform distribution of the scalar product between the unit vector defining the system position (denoted  $\mathbf{1}_*$  hereafter) and the unit vector defining the pole position (denoted  $\mathbf{1}_p$  hereafter). From Eq. (B.4), it is easy to verify that this scalar product  $\mathbf{1}_* \cdot \mathbf{1}_p$  equals  $-\cos i$ . Thus, an observational bias acting on our ability to derive the poles for systems with a given range of inclinations  $i$  would introduce a correlation between  $\mathbf{1}_*$  and  $\mathbf{1}_p$ . To check whether this is the case, we plot in Fig. 6 the distribution of  $\cos i$  values for all systems of Table 2 and for those with the poles analysed (thin line and shaded histogram). There is no significant difference between these distributions, meaning that the requirement of having radial velocities available for lifting the pole ambiguity does not introduce a selection bias on the orbital inclination  $i$ . On the other hand, the full-sample and pole-known distributions of  $\cos i$  are close to being uniform<sup>9</sup> except for two marginal peaks at 0.2 and 0.7. However, given the small amplitude of these peaks, it seems very unlikely that they could be at the origin of the segregation observed in the pole distribution. Furthermore, there is no obvious observational selection effect that we could think of that could cause peaks at  $\cos i \sim 0.2$  and 0.7.

<sup>9</sup> The maximum absolute difference between the uniform distribution and the distribution for pole-known systems is 0.11, which is not very significant (about 20% probability that such a difference be due to chance).

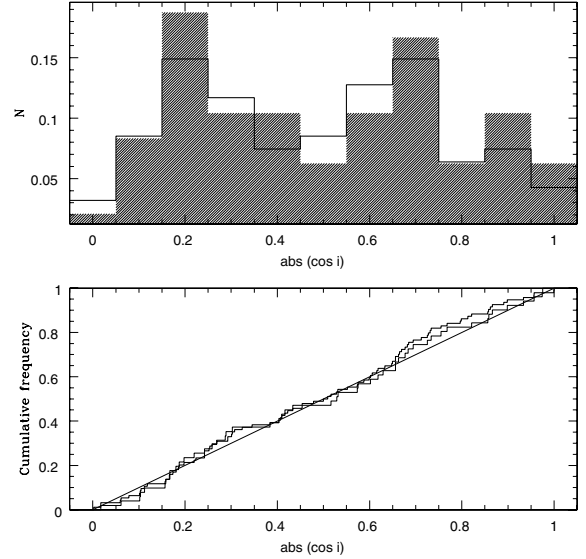


**Fig. 6.** Distribution of  $\cos i$  for all binaries from Table 2 (thick lines) and for those with the poles analysed (thin line in the bottom panel and shaded histogram in the upper panel).

## 6. Coplanarity in multiple systems

When searching for some anisotropy in the space orientation of orbital poles, which could either be signatures of the process of binary formation or of tidal effects from the Galactic disc, one could be misled by evolutionary processes acting within the stellar system itself that modify the orbital inclination. Within a triple system, weak perturbations from the outer body can have strong long-term effects on the inner binary. The simplest of these is precession of the orbital plane, which occurs if the orbital planes of the inner and outer binary are not aligned (Fabrycky & Tremaine 2007). If the inner and outer binary orbits are circular, this precession is analogous to the precession of two rigid rings with the same mass, radius, and angular momentum as the binary orbits; both the mutual inclination and the scalar angular momenta of the rings remain fixed, while the two angular momentum vectors precess around the direction defined by the total angular momentum vector of the triple system.

An unexpected aspect of this behaviour was discovered by (Kozai 1962; see also Kiseleva et al. 1998; Eggleton & Kiseleva-Eggleton 2001; Fabrycky & Tremaine 2007; Muterspaugh et al. 2008). Suppose the inner binary orbit is initially circular, with the initial mutual inclination between inner and outer binaries equal to  $i_{\text{initial}}$ . Kozai found that there is a critical angle  $i_c$  such that if  $i_{\text{initial}}$  is between  $i_c$  and  $180^\circ - i_c$ , then the orbit of the inner binary cannot remain circular as it precesses; both the eccentricity of the inner binary  $e_{\text{in}}$  and the mutual inclination  $i$  execute periodic oscillations known as Kozai cycles. The amplitude of the eccentricity and inclination oscillations is independent of the strength of the perturbation from the outer body (which depends on the mass of that outer body, and on  $a_{\text{out}}$  and  $e_{\text{out}}$ ), but the oscillation amplitude does depend on  $i_{\text{initial}}$ ; for initial circular orbits with  $i_{\text{initial}} = i_c$  or  $180^\circ - i_c$ , the eccentricity is 0, but if  $i_{\text{initial}} = 90^\circ$ , the highest eccentricity is unity, that is, the two inner bodies collide.

In the framework of the present study, it is important to stress that Kozai cycles occur independent of distances or component masses, their only requirement is that the mutual inclination is between  $i_c = 39.2^\circ$  and  $180^\circ - 39.2^\circ = 140.8^\circ$  (Fabrycky & Tremaine 2007; Muterspaugh et al. 2008).

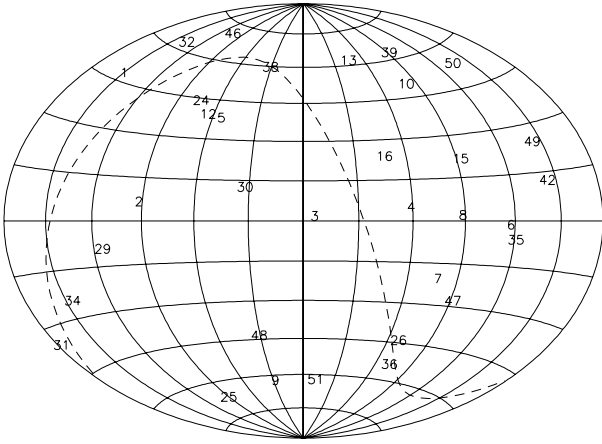


**Fig. 7.** Same as Fig. 1, but for the binary stars without indications for higher multiplicity.

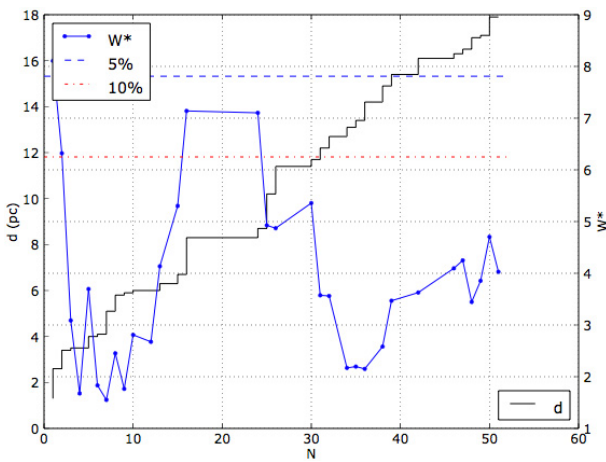


**Fig. 8.** Same as Fig. 3, but restricted to binary systems without evidence for higher multiplicity. The horizontal blue dashed and red dash-dotted curves correspond to a first-kind risk of 5% and 10%, respectively, of rejecting the null hypothesis of isotropy while it is true, based on the  $W^*$  statistics. The systems have the same number labels as in Table 3 and Fig. 3.

Hence, for triple systems, the current orbital pole may not at all be representative of its initial orientation if the Kozai mechanism is operating. Therefore, a discussion of the pole orientation should properly identify the triple systems, and possibly exclude them from the analysis. The triple and higher-multiplicity systems in our sample are identified by flag “t” in Tables 2 and 3, the notes in the Appendix provide more details in most cases.

Because the Kozai mechanism does alter the orbital inclinations of non-coplanar triple systems, we now investigate the pole-anisotropy problem separately for the sample devoid of triple systems (Figs. 7 and 8). These figures reveal that the Rayleigh-Watson test still predicts some deviation from isotropy in the sample restricted to 8 pc, but the first-kind error of the Rayleigh-Watson statistics this time is not better than 5%. We thus conclude that triple systems in the analysed sample do not degrade a possible anisotropy, quite the contrary, since the first-kind error of rejecting the null hypothesis of isotropy even increases when including the triple systems.

Nevertheless, the fact that several triple systems are now known not to be coplanar is certainly not in favour of a concentration of orbital poles on the celestial sphere. The quadruple system WDS 11182+3132 belongs to the sample of systems

closer than 8 pc to the Sun; the AB and Aa,Ab poles are known (Nos. 18 and 19 in Fig. 1) and are separated by about  $100^\circ$  on the sky. Although such a complete knowledge is not very frequent<sup>10</sup>, non-coplanarity is also observed in  $\eta$  Vir (HIP 60129: the orbital planes of the two systems are inclined by about  $30^\circ$  with respect to each other; Hummel et al. 2003), and similarly for the triple system V819 Her (HD 157482; O’Brien et al. 2011). In addition to V819 Her and  $\eta$  Vir, unambiguous mutual inclinations have been calculated for several other systems:  $\kappa$  Peg,  $\epsilon$  Hya,  $\zeta$  UMa, and Algol (see Table 5 of O’Brien et al. 2011, and references therein), and  $\mu$  Ori,  $\xi$  UMa,  $\epsilon$  Hya, and 88 Tau (Muterspaugh et al. 2008). These studies, along with the earlier ones by Fekel (1981) and Sterzik & Tokovinin (2002), strongly argued against coplanarity, despite predictions from older theories of formation of multiple stars (Bodenheimer 1978). Modern theories of stellar formation (Sterzik & Tokovinin 2002; Fabrycky & Tremaine 2007, and references therein) indeed predicted that triple systems will form non-coplanarily. Clearly, this result jeopardizes the possibility of observing coplanarity on a larger scale such as that of the solar neighbourhood. Therefore, the weak evidence for pole alignment observed in a sphere of 8 pc around the Sun does not receive support from our analysis of the properties of triple systems. In the next section, we show that neither do theories of binary-star formation coupled with the dispersive effect caused by Galactic rotation provide supportive arguments for a possible alignment of the orbital poles in the solar neighbourhood.

## 7. Pole alignment in the context of binary-star formation theories and Galactic kinematics

This section addresses the following two questions: (i) Do current theories of binary-star formation predict alignment of orbital poles for all binaries resulting from the same event of star formation; and (ii) assuming that the answer to the first question be positive, is this coherence in the pole orientation of young binary systems preserved by the Galactic kinematics in a volume-limited sample (the solar neighbourhood) consisting of much older systems?

Theories for wide and close binary-star formation have been reviewed by Bodenheimer & Burkert (2001) and Bonnell (2001), respectively. The favoured mechanism for producing most binary stellar systems is the fragmentation of a molecular cloud core during its gravitational collapse. Fragmentation can be divided into two main classes: direct fragmentation and rotational fragmentation (see references in Bate 2000). Direct fragmentation depends critically on the initial density structure within the molecular cloud core (e.g., non-spherical shape or density perturbations are needed to trigger the collapse), whereas rotational fragmentation is relatively independent of the initial density structure of the cloud because the fragmentation occurs due to non-axisymmetric instabilities in a massive, rotationally supported disc or ring. Not many studies of binary-star formation however include a discussion about the possible spatial alignment of the orbital poles of binary systems resulting from the same fragmentation event. This lack of information results from the difficulty of conducting the numerical simulations till the end of the binary formation, since a phase of accretion follows the initial fragmentation of the molecular cloud. To obtain the final

<sup>10</sup> Sterzik & Tokovinin (2002) revealed that there are only 22 triple systems with both orbits determined visually. Eight of these have questionable elements and only three have had their ascending nodes identified using radial velocity measurements.

parameters of a stellar system, the calculation must thus be performed until all of the original cloud material has been accumulated by one of the protostars or by their discs. Following simultaneously several among such events is an even more challenging task thus. Although [Bate \(2000\)](#) specifically investigated the properties of binary systems after this phase of accretion, there is no discussion whatsoever of the question of orbital-pole alignment. This was addressed in a very qualitative way by [Boss \(1988\)](#). A short discussion about the question of pole alignment has been found in the context of a variant of the fragmentation scenario, namely the shock-induced gravitational fragmentation followed by capture (SGF+C). That mechanism was initially proposed by [Pringle \(1989\)](#). Collisions between stable molecular cloud clumps produce dense shocked layers, which cool radiatively and fragment gravitationally. The resulting fragments then condense to form protostellar discs, which at the same time collapse and, as a result of tidal and viscous interactions, capture one another to form binary systems. When the initial clumps are sufficiently massive, a large number ( $>10$ ) of protostellar discs is produced. A prediction of the SGF+C mechanism ([Turner et al. 1995](#)) is that the resulting binary systems are likely to have their orbital and spin angular momenta aligned – the preferred direction of alignment being that of the global angular momentum of the original clump/clump pair. However, with more realistic, that is less highly organized, initial conditions, such alignments should still arise locally but are likely to be less well coordinated across large distances.

Even though there is currently no strong evidence from theories of binary formation for pole alignment in binary systems resulting from the same molecular-cloud collapsing event, we assumed for now such a coherence and followed what happened as a result of Galactic kinematics dispersing these coeval binary systems across the Galaxy. After several Galactic rotations, this coeval association will (fully or partly) evaporate and form a tube called supercluster. [Woolley \(1961\)](#) has presented an interesting argument that makes it possible to tag stars that formed at the same place and time, and that are still found together today in the solar neighbourhood. In general, stars found today in the solar neighbourhood emanate from various birth locations in the Galaxy because the diversity of stellar orbits in the Galaxy. Woolley’s argument goes as follows. Stars in the supercluster mentioned above still share common  $V$  velocities (with the usual notation  $(U, V, W)$  for the Galactic velocity components directed towards the Galactic centre, along the direction of Galactic rotation, and towards the north Galactic pole, respectively) when located in the same region of the tube (for example in the solar neighbourhood) for the following reason, as put forward by [Woolley \(1961\)](#): if the present Galactocentric radius of a star on a quasi-circular epicyclic orbit equals that of the Sun (denoted  $r_\odot$ ), and if such a star is observed with a peculiar velocity  $v = V + V_\odot$ , then its guiding-centre radius  $r_g$  writes

$$r_g = r_\odot - x_g = r_\odot + \frac{v}{2B}, \quad (18)$$

where  $x_g$  is the position of its guiding-centre in the Cartesian reference frame associated with the local standard of rest (LSR) (in the solar neighbourhood approximation, the impact of  $y_g$  is negligible), and  $B$  is the second Oort constant. [Woolley \(1961\)](#) pointed out that disc stars (most of which move on quasi-circular epicyclic orbits) that formed at the same place and time, and that because they stayed together in the Galaxy after a few galactic rotations (since they are all currently observed in the solar neighbourhood) must necessarily have the same period of revolution

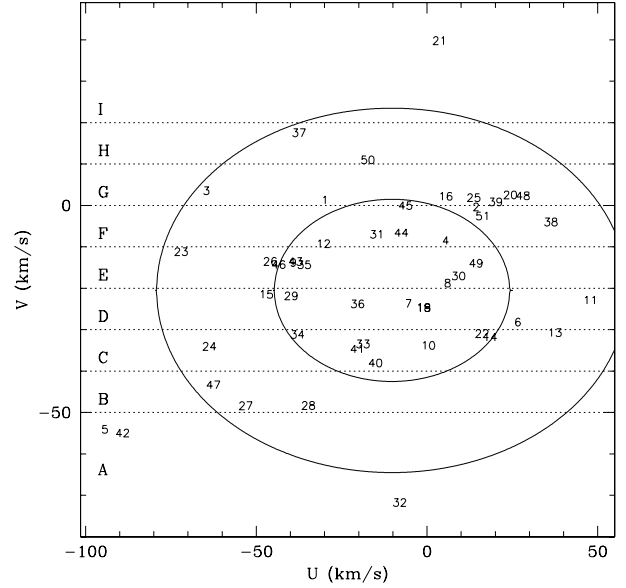


**Fig. 9.** Distribution of the systems in the  $(U, V)$  plane, with the same labels as in Fig. 1. System 17 (01083+5455) falls outside the boundaries, at  $U = -43$  km s $^{-1}$  and  $V = -157$  km s $^{-1}$ . To fix the ideas, two velocity ellipsoids are shown, both centred on the reflex solar motion in the LSR:  $-U_\odot = -10.2$  km s $^{-1}$ ,  $-V_\odot = -20.5$  km s $^{-1}$ , and with  $\sigma_U = 34.5$  km s $^{-1}$ ,  $\sigma_V = 22.5$  km s $^{-1}$ , as derived by [Famaey et al. \(2005\)](#) from their most precise sample. Horizontal bands and the corresponding labels are used in Fig. 10.

around the Galactic centre, and thus the same guiding-centre  $r_g$ , and thus the same velocity  $V = v - V_\odot$  according to Eq. (18).

Therefore, according to this argument, binary systems that formed in the same cluster or association and that stayed together after a few Galactic revolutions are observed today in the solar neighbourhood as sharing the same  $V$  velocity. In other words, if there are any orbital-pole concentrations on the celestial sphere that can be ascribed to angular momentum conservation for binary systems originating from the same cluster or association, they should be identified from similar  $V$  velocities.

We first computed the  $(U, V, W)$  velocity components from the HIPPARCOS proper motion and from the systemic velocity, according to standard prescriptions for converting equatorial to Galactic coordinates. The resulting distribution in the  $(U, V)$  plane is shown in Fig. 9.

As expected, the sample is distributed according to the general velocity ellipsoid, with overdensities observed at the location of the Sirius ( $\langle U \rangle \sim 6.5$  km s $^{-1}$ ,  $\langle V \rangle \sim 3.9$  km s $^{-1}$ ) and Hyades ( $\langle U \rangle \sim -40$  km s $^{-1}$ ,  $\langle V \rangle \sim -20$  km s $^{-1}$ ) streams (e.g., [Dehnen 1998](#); [Famaey et al. 2005](#)). Because of Woolley’s argument expressed above, the  $(U, V)$  diagram was divided into horizontal bands of width 10 km s $^{-1}$ , as indicated in Fig. 9, with a letter assigned to each of these  $V$ -bands. These letters were used to label the position of each pole on a Galactic-coordinate map (Fig. 10).

The absence of clustering of similar letters in restricted regions of the celestial sphere provides definite proof that any possible pole concentration on the sphere (see Sect. 4.3) cannot be traced back to a similar birth location for those systems. It must therefore either be ascribed to statistical fluctuations in our small-sized sample, or to some as yet unidentified physical process that removes orbital poles from the region  $90^\circ \leq l \leq 300^\circ$ ,  $b \leq 0^\circ$ , on a time scale of the order of that characterizing the

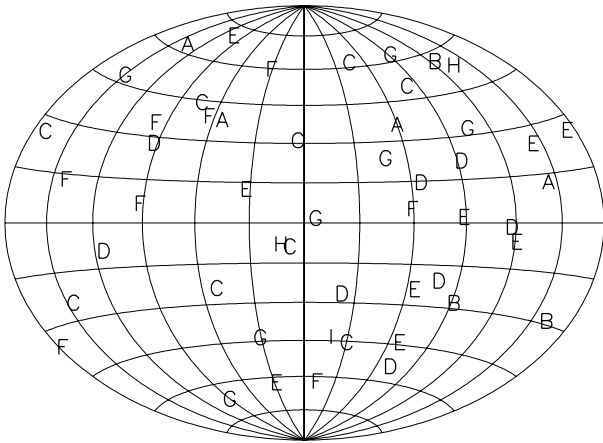


**Fig. 10.** Same as Fig. 1 but with a letter coding the value of the galactic  $V$  velocity (see Fig. 9). A necessary condition for binary systems to originate from the same cluster/association at birth is to have similar  $V$  velocities (see text), hence they should be labelled by the same letter.

convergence of systems with different Galactic orbits in the solar neighbourhood. Our Galaxy being in general symmetric with respect to its equatorial plane, it is however difficult to imagine a physical process that would break such a symmetry (the fact that the Sun lies somewhat above the Galactic plane? see below), as it seems to be required to account for the observed asymmetry.

Conversely, the poles of the binary systems belonging to the Sirius or Hyades streams do not concentrate either on the sphere, which is a further confirmation that these streams are not evaporated clusters, but rather have a dynamical origin (Famaey et al. 2005, 2007, 2008; Pompéia et al. 2011).

Finally, one should mention, for the sake of completeness, that the location of the Sun slightly above the Galactic plane ( $\sim 20$  pc; Humphreys & Larsen 1995) could be responsible for the (Galactic) North–South asymmetry observed in the orbital-pole distribution, if some effect related to Galactic tides were the cause of the pole anisotropy. That seems unlikely, however, given the low intensity of Galactic tides with respect to the two-body interaction. Heisler & Tremaine (1986) have expressed Galactic tides in terms of the Oort constants. Based on the size of the last closed Hill surface<sup>11</sup>, they conclude that in the solar neighbourhood, the Galactic tides have a non-negligible impact only on systems with semi-major axes of several  $10^4$  AU (such as Oort-cloud comets around the Sun). The binary systems defining the pole statistics are very much tighter than this, so that there seems to be no way for the Galactic tides to imprint their signature on the orbital-pole distribution.

## 8. Conclusion

Among the 95 systems with an orbit in the 6th Catalogue of Orbits of Visual Binaries that are closer than 18 pc from the Sun, we were able to lift the pole ambiguity for 51 systems, thanks to radial-velocity data either collected from the literature, obtained from the CORAVEL database, or acquired with the HERMES/Mercator spectrograph. Of these 51 systems, several had an erroneous node choice listed in the 6th USNO orbit catalogue and had thus to be corrected. An interesting side product of the present study is a number of new spectroscopic orbits obtained from CORAVEL and HERMES radial velocities,

<sup>11</sup> The Hill (or zero-velocity) surface is defined as the surface on which the Jacobi integral of the restricted three-body problem is constant.

as well as new combined spectroscopic/astrometric orbits for seven systems (WDS 01083+5455aa,Ab; 01418+4237AB; 02278+0426AB (SB2); 09006+4147AB (SB2); 16413+3136AB; 17121+4540AB; 18070+3034AB).

This new sample of 51 orbital poles was subjected to several methods of spherical statistics (Rayleigh-Watson, Bingham, Beran and Giné) to test possible deviations from isotropy. After ordering the binary systems by increasing distance from the Sun, the false-alarm probability (of rejecting the null hypothesis of isotropy while it is true) was computed for subsamples of increasing sizes, from  $N = 1$  up to the full sample of 51 systems. Two tests (Rayleigh-Watson’s and Beran’s) delivered a false-alarm probability of 0.5% when considering the subsample of 21 systems closer than 8.1 pc to the Sun. The poles tend to cluster toward Galactic position  $l = 46^\circ$ ,  $b = 37^\circ$ . This direction is not so distant from that of the ecliptic pole ( $l = 96^\circ$ ,  $b = 30^\circ$ ). To evaluate the robustness of this clustering, a jack-knife approach was used by repeating the above procedure after removing one system at a time from the full sample. The above false-alarm probability was then found to vary between 1.5% and 0.1%, depending on which system is removed from the sample. The reality of the deviation from isotropy can thus not be assessed with certainty at this stage, given the small number of systems available, despite our efforts to increase it. Our so far uncertain conclusion should be seen as an incentive to foster further studies on this problem, especially in the Gaia era.

For the full sample extending up to 18 pc, the clustering totally vanishes (the Rayleigh-Watson first-kind risk then rises to 18%). If present, coplanarity of orbits must thus be restricted to small spheres with a radius of the order of 10 pc, but several dynamical arguments were presented to show that the physical origin of any such coplanarity, should it exist, will be difficult to identify. In this context, the recent result of Rees & Zijlstra (2013) on the non-random orientation of *bipolar* planetary nebulae in the Galactic Bulge, using a statistical method much like the ones used in our present study, came as a surprise. Rees & Zijlstra found evidence for an anisotropy in the orientation of the bipolar planetary nebulae, whose specific geometry is usually attributed to the binarity of the central star. Assuming that the symmetry axis of the bipolar nebula coincides with the polar axis of the orbit, the result of Rees & Zijlstra is therefore indirect evidence of a deviation from anisotropy for the poles of a subsample of binaries in the Galactic Bulge. The physical explanation proposed for the Galactic Bulge (related to the impact of the Galactic magnetic field on the binary formation process) is, however, unlikely to hold also for the solar neighbourhood, where the field is of lower intensity.

*Acknowledgements.* We dedicate this paper to the memory of J. Dommangeat, who initiated this study and could unfortunately not see it accomplished. He would certainly have preferred a more significant result, but he had faith in statistics.

We thank the anonymous referee for his constructive remarks and attitude. We thank A. Lobel, P. Neykens and C. Siopis, who acted as observers on the HERMES spectrograph and secured the necessary spectra to solve the pole ambiguity for several binary systems. Based on observations made with the *Mercator* Telescope, operated on the island of La Palma by the Flemish Community, at the Spanish Observatorio del Roque de los Muchachos of the Instituto de Astrofísica de Canarias. Based on observations obtained with the HERMES spectrograph, which is supported by the Fund for Scientific Research of Flanders (FWO), Belgium, the Research Council of K.U. Leuven, Belgium, the Fonds National de la Recherche Scientifique (FNRS), Belgium, the Royal Observatory of Belgium, the Observatoire de Genève, Switzerland and the Thüringer Landessternwarte Tautenburg, Germany. We gratefully thank D. Pourbaix (Institut d’Astronomie et d’Astrophysique de l’Université Libre de Bruxelles) for his help in the calculation of the new orbits, as well as G. Marcy for sharing his velocity measurements of WDS 00057+4549AB. This research has made use of the Simbad database,

operated at the Centre de Données Astronomiques de Strasbourg (CDS), France. Available at <http://cdsweb.u-strasbg.fr/>. This research has made use of the Washington Double Star Catalog maintained at the US Naval Observatory. Available at <http://ad.usno.navy.mil/wds/>.

## References

- Abt, H. A. 1965, *ApJS*, 11, 429  
 Abt, H. A., & Levy, S. G. 1976, *ApJS*, 30, 273  
 Abt, H. A., & Willmarth, D. 2006, *ApJS*, 162, 207  
 Aitken, R. G. 1918, *Lick Observatory Bull.*, 9, 184  
 Anderson, T. W., & Stephens, M. A. 1972, *Biometrika*, 59, 613  
 Andrade, M. 2007, *Rev. Mex. Astron. Astrofis.*, 43, 237  
 Baize, P. 1976, *A&AS*, 26, 177  
 Baize, P. 1980, *Inf. Circ. IAU Comm.*, 26, 80  
 Balega, I. I., Balega, Y. Y., Hofmann, K.-H., et al. 2005, *A&A*, 433, 591  
 Baranne, A., Mayor, M., & Poncet, J. L. 1979, *Vistas in Astron.*, 23, 279  
 Barry, R. K., Demory, B.-O., Ségransan, D., et al. 2012, *ApJ*, 760, 55  
 Bate, M. R. 2000, *MNRAS*, 314, 33  
 Batten, A. H. 1967, in *Determination of Radial Velocities and their Applications*, eds. A. H. Batten, & J. F. Heard, *IAU Symp.*, 30, 199  
 Benedict, G. F., McArthur, B. E., Franz, O. G., et al. 2001, *AJ*, 121, 1607  
 Beran, R. J. 1968, *J. Appl. Probab.*, 5, 177  
 Bertiau, F. C. 1957, *ApJ*, 125, 696  
 Beuzit, J.-L., Ségransan, D., Forveille, T., et al. 2004, *A&A*, 425, 997  
 Bingham, C. 1974, *Ann. Stat.*, 2, 1201  
 Bodenheimer, P. 1978, *ApJ*, 224, 488  
 Bodenheimer, P., & Burkert, A. 2001, in *The Formation of Binary Stars*, eds. H. Zinnecker, & R. Mathieu, *IAU Symp.*, 200, 13  
 Bonnell, I. A. 2001, in *The Formation of Binary Stars*, eds. H. Zinnecker, & R. Mathieu, *IAU Symp.*, 200, 23  
 Boss, A. P. 1988, *Comm. Astrophys.*, 12, 169  
 Briggs, M. S. 1993, *ApJ*, 407, 126  
 Chang, K. 1972, *AJ*, 77, 759  
 Christie, W. H. 1934, *ApJ*, 80, 181  
 Chubak, C., Marcy, G., Fischer, D. A., et al. 2012 [[arXiv:1207.6212](https://arxiv.org/abs/1207.6212)]  
 Couteau, P. 1960, *Bull. Astron. Paris*, 23, 127  
 Cox, A. N. 2000, *Allen's Astrophysical Quantities* (New York: Springer)  
 Cvetković, Z., Pavlović, R., Ninković, S., & Stojanović, M. 2012, *AJ*, 144, 80  
 Dahn, C. C., Harrington, R. S., Kallarakal, V. V., et al. 1988, *AJ*, 95, 237  
 Dehnen, W. 1998, *AJ*, 115, 2384  
 Delfosse, X., Forveille, T., Perrier, C., & Mayor, M. 1998, *A&A*, 331, 581  
 Delfosse, X., Forveille, T., Ségransan, D., et al. 2000, *A&A*, 364, 217  
 Docobo, J. A., & Costa, J. M. 1985, *IAU Commission on Double Stars*, 96, 1  
 Docobo, J. A., & Ling, J. F. 2010, *IAU Commission on Double Stars*, 171, 1  
 Docobo, J. A., Tamazian, V. S., Balega, Y. Y., et al. 2008, *A&A*, 478, 187  
 Dommanget, J. 1968, *Bull. Astron. Obs. Royal Belgique*, 6, 246  
 Dommanget, J. 1978, *Bull. Astron. Obs. Royal Belgique*, 9, 47  
 Dommanget, J. 1988, *Astrophys. Space Sci.*, 142, 171  
 Dommanget, J. 2005, *Ciel et Terre*, 121, 2  
 Dommanget, J. 2014, *Observations et Travaux*, submitted  
 Dommanget, J., & Nys, O. 2006, *Observations et Travaux*, 62, 5  
 Drummond, J. D., Christou, J. C., & Fugate, R. Q. 1995, *ApJ*, 450, 380  
 Dufflot, M., Figon, P., & Meyssonnier, N. 1995, *A&AS*, 114, 269  
 Duquennoy, A., & Mayor, M. 1991, *A&A*, 248, 485  
 Duquennoy, A., Mayor, M., & Halbwachs, J.-L. 1991, *A&AS*, 88, 281  
 Eggen, O. J. 1956, *AJ*, 61, 405  
 Eggenberger, P., Miglio, A., Carrier, F., Fernandes, J., & Santos, N. C. 2008, *A&A*, 482, 631  
 Eggleton, P. P., & Kiseleva-Eggleton, L. 2001, *ApJ*, 562, 1012  
 ESA 1997, *The Hipparcos and Tycho Catalogues*, ESA SP (Noordwijk: ESA publications Division), 1200  
 ESA 1997, *VizieR Online Data Catalog I/239*  
 Fabrycky, D., & Tremaine, S. 2007, *ApJ*, 669, 1298  
 Famaey, B., Jorissen, A., Luri, X., et al. 2005, *A&A*, 430, 165  
 Famaey, B., Pont, F., Luri, X., et al. 2007, *A&A*, 461, 957  
 Famaey, B., Siebert, A., & Jorissen, A. 2008, *A&A*, 483, 453  
 Farrington, C. D., ten Brummelaar, T. A., Mason, B. D., et al. 2010, *AJ*, 139, 2308  
 Fekel, Jr., F. C. 1981, *ApJ*, 246, 879  
 Fekel, F. C., & Tomkin, J. 1983, *PASP*, 95, 1000  
 Fekel, Jr., F., Lacy, C. H., & Bopp, B. W. 1978, *AJ*, 83, 1445  
 Finsen, W. S. 1933, *Circular of the Union Observatory Johannesburg*, 90, 397  
 Finsen, W. S. 1934, *Circular of the Union Observatory Johannesburg*, 91, 23  
 Fisher, R. 1953, *Proc. Roy. Soc. A*, 217, 295  
 Forveille, T., Beuzit, J.-L., Delfosse, X., et al. 1999, *A&A*, 351, 619  
 Franz, O. G., Wasserman, L. H., Benedict, G. F., et al. 1999, in *Working on the Fringe: Optical and IR Interferometry from Ground and Space*, eds. S. Unwin, & R. Stachnik, *ASP Conf. Ser.*, 194, 28  
 Gatewood, G. 2005, *AJ*, 130, 809  
 Genova, F., Egret, D., Bienaymé, O., et al. 2000, *A&AS*, 143, 1  
 Geyer, D. W., Harrington, R. S., & Worley, C. E. 1988, *AJ*, 95, 1841  
 Gillett, S. L. 1988, *AJ*, 96, 1967  
 Giné, M. E. 1975, *Ann. Stat.*, 3, 1243  
 Girard, T. M., Wu, H., Lee, J. T., et al. 2000, *AJ*, 119, 2428  
 Gizis, J. E., Reid, I. N., & Hawley, S. L. 2002, *AJ*, 123, 3356  
 Glebocki, R. 2000, *Acta Astron.*, 50, 211  
 Gorshanov, D. L., Shakht, N. A., & Kisselev, A. A. 2006, *Astrophys.*, 49, 386  
 Griffin, R. F. 1998, *The Observatory*, 118, 273  
 Griffin, R. F. 2004, *The Observatory*, 124, 258  
 Griffin, R. F., & Emerson, B. 1975, *The Observatory*, 95, 23  
 Hale, A. 1994, *AJ*, 107, 306  
 Han, I., & Gatewood, G. 2002, *PASP*, 114, 224  
 Hartkopf, W. I., & Mason, B. D. 2003, *IAU Commission on Double Stars*, 151, 2  
 Hartkopf, W. I., Mason, B. D., & McAlister, H. A. 1996, *AJ*, 111, 370  
 Hartkopf, W. I., Mason, B. D., & Worley, C. E. 2001, *AJ*, 122, 3472  
 Hartmann, D., & Epstein, R. I. 1989, *ApJ*, 346, 960  
 Heintz, W. D. 1967, *Veröff. Sternw. München*, 7, 31  
 Heintz, W. D. 1974, *AJ*, 79, 819  
 Heintz, W. D. 1984, *AJ*, 89, 1063  
 Heintz, W. D. 1986, *A&AS*, 65, 411  
 Heintz, W. D. 1987, *PASP*, 99, 1084  
 Heintz, W. D. 1988, *A&AS*, 72, 543  
 Heintz, W. D. 1990a, *A&AS*, 82, 65  
 Heintz, W. D. 1990b, *AJ*, 99, 420  
 Heintz, W. D. 1994, *AJ*, 108, 2338  
 Heintz, W. D. 1996, *AJ*, 111, 408  
 Heintz, W. D., & Cantor, B. A. 1994, *PASP*, 106, 363  
 Heisler, J., & Tremaine, S. 1986, *Icarus*, 65, 13  
 Hinkley, S., Monnier, J. D., Oppenheimer, B. R., et al. 2011, *ApJ*, 726, 104  
 Hopmann, J. 1958, *Mitteilungen der Universitaets-Sternwarte Wien*, 9, 177  
 Hopmann, J. 1973, *Mitteilungen der Universitaets-Sternwarte Wien*, 14, 18  
 Hummel, C. A., Benson, J. A., Hutter, D. J., et al. 2003, *AJ*, 125, 2630  
 Humphreys, R. M., & Larsen, J. A. 1995, *AJ*, 110, 2183  
 Irwin, A. W., Yang, S. L. S., & Walker, G. A. H. 1996, *PASP*, 108, 580  
 Jancart, S., Jorissen, A., Babusiaux, C., & Pourbaix, D. 2005, *A&A*, 442, 365  
 Johnson, D. R. H., & Soderblom, D. R. 1987, *AJ*, 93, 864  
 Kamper, K. W., & Beardsley, W. R. 1986, *AJ*, 91, 419  
 Kamper, K. W., Legget, D., & McCarthy, Jr., D. W. 1989, *AJ*, 98, 686  
 Keilson, J., Petronidas, D., Sumita, U., & Wellner, J. 1983, *J. Statistical Computation and Simulation*, 17, 195  
 Kirkpatrick, J. D., Gelino, C. R., Cushing, M. C., et al. 2012, *ApJ*, 753, 156  
 Kiseleva, L. G., Eggleton, P. P., & Mikkola, S. 1998, *MNRAS*, 300, 292  
 Kiyavea, O. V., Kisselev, A. A., Polyakov, E. V., & Rafal'Skii, V. B. 2001, *Sov. Astron. Lett.*, 27, 391  
 Konacki, M., Muterspaugh, M. W., Kulkarni, S. R., & Helminiak, K. G. 2010, *ApJ*, 719, 1293  
 Kozai, Y. 1962, *AJ*, 67, 591  
 Kroupa, P., Tout, C. A., & Gilmore, G. 1993, *MNRAS*, 262, 545  
 Lippincott, S. L. 1967, *AJ*, 72, 1349  
 Lippincott, S. L. 1972, *AJ*, 77, 165  
 Lippincott, S. L. 1981, *ApJ*, 248, 1053  
 Lippincott, S. L., Braun, D., & McCarthy, Jr., D. W. 1983, *PASP*, 95, 271  
 Lu, W., Rucinski, S. M., & Ogłóza, W. 2001, *AJ*, 122, 402  
 Madler, J. H. 1838, *C. R. Acad. Sci.*, 6, 290  
 Mante, R. 2000, *IAU Commission on Double Stars*, 140, 1  
 Mardia, K., & Jupp, P. 2000, *Directional statistics* (New York: Wiley)  
 Martin, C., & Mignard, F. 1998, *A&A*, 330, 585  
 Martinache, F., Lloyd, J. P., Ireland, M. J., Yamada, R. S., & Tuthill, P. G. 2007, *ApJ*, 661, 496  
 Mason, B. D., & Hartkopf, W. I. 2011, *IAUDS*, 174, 1  
 Mason, B. D., McAlister, H. A., Hartkopf, W. I., & Shara, M. M. 1995, *AJ*, 109, 332  
 Mason, B. D., Douglass, G. G., & Hartkopf, W. I. 1999, *AJ*, 117, 1023  
 Mazeh, T., Latham, D. W., Goldberg, E., et al. 2001, *MNRAS*, 325, 343  
 McCarthy, Jr., D. W. 1983, in *IAU Colloq. Nearby Stars and the Stellar Luminosity Function*, eds. A. G. D. Philip, & A. R. Uppgren, 76, 107  
 Muterspaugh, M. W., Lane, B. F., Fekel, F. C., et al. 2008, *AJ*, 135, 766  
 Muterspaugh, M. W., Hartkopf, W. I., Lane, B. F., et al. 2010a, *AJ*, 140, 1623  
 Muterspaugh, M. W., Lane, B. F., Kulkarni, S. R., et al. 2010b, *AJ*, 140, 1631  
 Muterspaugh, M. W., Lane, B. F., Kulkarni, S. R., et al. 2010c, *AJ*, 140, 1657  
 Nidever, D. L., Marcy, G. W., Butler, R. P., Fischer, D. A., & Vogt, S. S. 2002, *ApJS*, 141, 503

- O'Brien, D. P., McAlister, H. A., Raghavan, D., et al. 2011, *ApJ*, 728, 111  
 Pompéia, L., Masseron, T., Famaey, B., et al. 2011, *MNRAS*, 415, 1138  
 Popovic, G. M., & Pavlovic, R. 1996, *Bull. Obs. Astron. Beograd*, 153, 57  
 Pourbaix, D. 2000, *A&AS*, 145, 215  
 Pourbaix, D., Nidever, D., McCarthy, C., et al. 2002, *A&A*, 386, 280  
 Pourbaix, D., Tokovinin, A. A., Batten, A. H., et al. 2004, *A&A*, 424, 727  
 Pringle, J. E. 1989, *MNRAS*, 239, 361  
 Raghavan, D., McAlister, H. A., Henry, T. J., et al. 2010, *ApJS*, 190, 1  
 Raskin, G., van Winckel, H., Hensberge, H., et al. 2011, *A&A*, 526, A69  
 Rees, B., & Zijlstra, A. A. 2013, *MNRAS*, 435, 975  
 Reid, I. N., Hawley, S. L., & Gizis, J. E. 1995, *AJ*, 110, 1838  
 Rica Romero, F. M. 2008, *IAU Commission on Double Stars*, 165, 1  
 Russell, J. L., & Gatewood, G. D. 1984, *PASP*, 96, 429  
 Scardia, M. 2002, *IAU Commission on Double Stars*, 148, 1  
 Scardia, M., Argyle, R. W., Prieur, J.-L., et al. 2007, *Astron. Nachr.*, 328, 146  
 Scardia, M., Prieur, J.-L., Pansecchi, L., et al. 2008, *Astron. Nachr.*, 329, 54  
 Scarfe, C. D., Funakawa, H., Delaney, P. A., & Barlow, D. J. 1983, *J. Roy. Astron. Soc. Can.*, 77, 126  
 Ségransan, D., Delfosse, X., Forveille, T., et al. 2000, *A&A*, 364, 665  
 Seymour, D. M., Mason, B. D., Hartkopf, W. I., & Wycoff, G. L. 2002, *AJ*, 123, 1023  
 Söderhjelm, S. 1999, *A&A*, 341, 121  
 Stephens, M. 1964, *J. Amer. Statist. Assn.*, 59, 160  
 Sterzik, M. F., & Tokovinin, A. A. 2002, *A&A*, 384, 1030  
 Strand, K. A. 1969, *AJ*, 74, 760  
 Strand, K. A. 1977, *AJ*, 82, 745  
 ten Brummelaar, T., Mason, B. D., McAlister, H. A., et al. 2000, *AJ*, 119, 2403  
 Tokovinin, A. 2008, *MNRAS*, 389, 925  
 Tokovinin, A. A., & Smekhov, M. G. 2002, *A&A*, 382, 118  
 Tokovinin, A., Kiyaveva, O., Sterzik, M., et al. 2005, *A&A*, 441, 695  
 Turner, J. A., Chapman, S. J., Bhattal, A. S., et al. 1995, *MNRAS*, 277, 705  
 Underhill, A. B. 1963, *Publ. DAO*, 12, 159  
 Upton, G., & Fingleton, B. 1989, *Spatial Data Analysis by Example (New York: Wiley)*, 2  
 van Albada, G. B. 1957, *Contributions from the Bosscha Observatory*, 5, 1  
 van den Bos, W. H. 1960, *J. Observateurs*, 43, 145  
 van Leeuwen, F. 2007, *A&A*, 474, 653  
 Vinter Hansen, J. M., Neubauer, F. J., & Roosen-Raad, D. 1940, *Lick Observatory Bulletin*, 19, 89  
 Watson, G. 1956, *Geophys. J. Int.*, 7, 160  
 Watson, G. 1966, *J. Geology*, 74, 786  
 Watson, G. 1983, *Statistics on Spheres (New York: Wiley)*  
 Wieth-Knudsen, N. 1957, *IAU Commission on Double Stars*, 13, 1  
 Woolley, R. 1961, *The Observatory*, 81, 203  
 Zirm, H. 2003, *IAU Commission on Double Stars*, 151, 1  
 Zirm, H. 2011, *J. Double Star Observations*, 7, 24

**Table 1.** Cross-identifications for the master list of 95 systems closer than 20 pc from the Sun and the are known to have an orbit in the 6th COVBS at USNO.

WDS	CCDM	HIP/HIC	HD	SB9	Name
00022+2705AB	00022+2705AB	171	224930	1468	BU 733
00057+4549AB	00057+4549AB	473	38		STT 547
00184+4401AB	00184+4401AB	1475	1326		GRB 34
00321+6715Aa,Ab	00325+6714A	2552	–	–	MCY 1
00321+6715AB	00325+6714AB	2552	–	–	VYS 2
00373-2446AB	00373-2446AB	2941	3443	–	BU 395
00491+5749AB	00491+5749AB	3821	4614	–	STF 60
01032+2006AB	01032+2006AB	4927	–	–	LDS 873
01083+5455Aa,Ab	01080+5455A	5336	6582	57	WCK 1
01388-1758AB	01390-1756AB	–	–	–	LDS 838
01398-5612AB	01398-5612AB	7751	10360	–	DUN 5
01418+4237AB	01418+4237AB	7918	10307	2546	MCY 2
01425+2016AB	01425+2016AB	7981	10476	–	HJ 2071
02171+3413Aa,Ab	02170+3414A	10644	13974	117	MKT
02278+0426AB	02278+0426AB	11452	15285	–	A 2329
02361+0653Aa,P	02361+0653A	12114	16160	–	PLQ 32
02442+4914AB	02441+4913AB	12777	16895	–	STF 296
03095+4544AB	03095+4544AB	14669	–	–	HDS 404
03121-2859AB	03121-2859AB	14879	20010	–	HJ 3555
03575-0110AB	03575-0110AB	18512	24916	–	BU 543
04153-0739BC	04153-0739BC	–	26976	–	STF 518
04312+5858Aa,Ab	04312+5858A	21088	–	–	STN 2051
05025-2115AB	05025-2115AB	23452	32450	–	DON 91
05074+1839AB	05075+1839AB	23835	32923	–	A 3010
05167+4600Aa,Ab	05168+4559AP	24608	34029	306	ANJ 1
05333+4449	05333+4449A	–	–	–	GJ 1081
05544+2017	05544+2017A	27913	39587	1535	$\chi^1$ Ori
06003-3102AC	06003-3102AC	28442	40887	–	HJ 3823
06262+1845AB	06262+1845AB	30630	45088	–	BU 1191
06293-0248AB	06294-0249AB	30920	–	–	B 2601
06451-1643AB	06451-1643AB	32349	48915	416	AGC 1
06579-4417AB	06578-4417AB	33499	–	–	LPM 248
07100+3832	–	34603	–	434	GJ 268
07175-4659AB	07175-4659AB	35296	57095	–	I 7
07346+3153AB	07346+3153AB	36850	60178/9	–	STF 1110
07393+0514AB	07393+0514AB	37279	61421	467	SHB 1
07518-1354AB	07518-1354AB	38382	64096	478	BU 101
08592+4803A,BC	08592+4803AB	44127	76644	–	HJ 2477
09006+4147AB	09007+4147AB	44248	76943	546	KUI 37
09144+5241AB	09144+5241AB	45343	79210	–	STF 1321
09313-1329AB	09313-1329AB	46706	–	–	KUI 41
09357+3549AB	09357+3549AB	47080	82885	–	HU 1128
10454+3831AB	10454+3831AB	52600	–	–	HO 532
11182+3132AB	11182+3132AB	–	98231	–	STF 1523
11182+3132Aa,Ab	11182+3132A	–	98231	–	$\xi$ UMa
11247-6139AB	11247-6139AB	55691	99279	–	BSO 5
12417-0127AB	12417-0127AB	61941	110380	–	STF 1670
13100+1732AB	13100+1732AB	64241	114378	–	STF 1728
13169+1701AB	13169+1701AB	64797	115404	–	BU 800
13198+4747AB	13198+4747AB	65026	115953	–	HU 644
13328+1649AB	13328+1649AB	66077	–	–	VYS 6
13473+1727AB	13473+1727AB	67275	120136	–	STT 270
13491+2659AB	13491+2659AB	67422	120476	–	STF 1785
13547+1824	13547+1824A	67927	121370	794	$\eta$ Boo
14035+1047	14035+1047A	68682	122742	799	GJ 538

**Notes.** The column labelled “SB9” lists the entry number in the 9th Catalogue of Spectroscopic Binary Orbits (Pourbaix et al. 2004).

Table 1. continued.

WDS	CCDM	HIP/HIC	HD	SB9	Name
14396-6050AB	14396-6050AB	71683	128620	815	RHD
14514+1906AB	14513+1906AB	72659	131156	–	STF 1888
14540+2335AB	14539+2333AB	72896	–	–	REU 2
14575-2125AB	14574-2124AB	73184	131977	–	H N 28
14575-2125Ba,Bb	14574-2124B	73182	131976	1475	H N 28B
15038+4739AB	15038+4739AB	73695	133640	–	STF 1909
15232+3017AB	15233+3018AB	75312	137107	842	STF 1937
15527+4227	15527+4227A	77760	142373	–	$\chi$ Her
16240+4822Aa,Ab	16240+4821A	80346	–	1542	HEN 1
16413+3136AB	16413+3136AB	81693	150680	915	STF 2084
16555-0820AB	16555-0820AB	82817	152751	2683	KUI 75
17121+4540AB	17121+4540AB	84140	155876	–	KUI 79
17153-2636AB	17155-2635AB	84405	155885/6	–	SHJ 243
17190-3459AB	17190-3459AB	84709	156384	–	MLO 4
17191-4638AB	17191-4638AB	84720	156274	–	BSO 13
17304-0104AB	17304-0104AB	85667	158614	969	STF 2173
17349+1234	17349+1234A	86032	159561	–	MCY 4
17350+6153AB	17351+6152AB	86036	160269	2557	BU 962
17364+6820Aa,Ab	17366+6822A	86162	–	–	CHR 62
17465+2743BC	17465+2744BC	86974	161797	–	AC 7
18055+0230AB	18055+0230AB	88601	165341	1122	STF 2272
18070+3034AB	18071+3034AB	88745	165908	–	AC 15
18211+7244Aa,Ab	18211+7245A	89937	170153	1058	LAB 5
18428+5938AB	18428+5938A	91768	173739	–	STF 2398
18570+3254AB	18570+3254AB	93017	176051	2259	BU 648
19074+3230Ca,Cb	19075+3231C	–	–	–	KUI 90
19121+0254AB	19122+0253A	94349	–	–	AST 1
19167-4553AB	19167-4553AB	94739	179930	–	RST 4036
19255+0307Aa,Ab	19254+0307A	95501	182640	–	BNU 6
20452-3120BC	–	102141	196982	–	LDS 720
21000+4004AB	21001+4004A	103655	–	1280	KUI 103
21069+3845AB	21069+3844AB	104214	201091/2	–	STF 2758
21313-0947AB	21313-0947AB	106255	–	–	BLA 9
21379+2743Aa,Ab	21380+2743A	106811	–	–	HDS 3080
22070+2521	22070+2520A	109176	210027	1354	$\iota$ Peg
22234+3228AB	22235+3228AB	110526	–	–	WOR 11
22280+5742AB	22281+5741AB	110893	239960	–	KR 60
22385-1519AB	–	–	–	–	BLA 10
23317+1956AB	23319+1956AB	116132	–	–	WIR 1
23524+7533AB	23526+7532AB	117712	223778	–	BU 996

Table 2. Data and references for the 95 systems of the master list.

WDS	$\varpi$ (mas)	Sp	$P$ (yr)	$a$ ( $''$ )	$M_{\text{tot}}$ ( $M_{\odot}$ )	$\frac{M_b}{M_A}$	Gr	V.Orb.	S.Orb.	A	Notes
00022+2705AB	82.2	G5 Vb	26.27	0.83	1.49	–	2	Sod1999	Gri2004	Y	–
00057+4549AB	88.4	K6 V	509.7	6.21	1.33	–	4	Kiy2001	SD	Y	nt
00184+4401AB	278.8	M2.0V	2600	41.15	0.48	–	5	Lip1972	–	NO, ND	n
00321+6715Aa,Ab	99.3	M2.5Ve	15.64	0.511	0.56	–	4	Doc2008d	–	NV	t
00321+6715AB	99.3	M2.5Ve	222.3	3.322	0.76	–	5	Doc2008d	–	NV	nt
00373-2446AB	64.9	G8V+G8V	25.09	0.667	1.72	–	1	Pbx2000b	Pbx2000b	Y	–
00491+5749AB	168.0	G3V	480	11.99	1.58	–	3	Str1969a	VD	Y	–
01032+2006AB	61.6	M2	521.4	3.366	0.60	–	4	FMR2008b	–	NV	–
01083+5455Aa,Ab	132.4	G5Vb	21.75	1.009	0.94	–	4	Dru1995	New	Y	nt
01388-1758AB	373.7	M5.5V+M6.0V	26.52	1.95	0.20	–	3	USN1988b	–	NV	–
01398-5612AB	127.8	K0V+K5V	483.6	7.817	0.98	–	5	vAb1957	–	NO, ND	n
01418+4237AB	78.5	G1.5V	19.5	0.58	1.06	–	4	New	New	Y	n
01425+2016AB	132.8	K1V	0.567	0.005	–	–	9	HIP1997d	–	ND	n
02171+3413Aa,Ab	92.7	G0.5V	0.027	0.010	1.57	0.89	1	Pbx2000b	Pbx2000b	Y	t
02278+0426AB	58.3	M1V	25.14	0.543	1.80	0.89	1	New	New	Y	n
02361+0653Aa,P	139.3	K3V	61.0	0.171	–	–	9	Hei1994b	–	ND	nt
02442+4914AB	89.9	F7V	2720	22.29	2.06	–	5	Hop1958	–	NO, ND	n
03095+4544AB	63.4	M2	28.31	0.569	0.90	–	4	Bag2005	–	NV	–
03121-2859AB	70.2	F6V	269.0	4.00	2.55	–	4	Sod1999	VD	Y	–
03575-0110AB	64.4	K4V	3200	11.1	0.50	–	5	Dom1978	–	NO, ND	n
04153-0739BC	198.2	DA	252.1	6.943	0.68	–	4	Hei1974c	–	NO, ND	nt
04312+5858Aa,Ab	179.3	M4	23.0	0.070	–	–	9	Str1977	–	NV	nt
05025-2115AB	116.6	M0V	44.0	1.80	1.90	–	4	Sod1999	–	NV	–
05074+1839AB	64.8	G4V	1.19	0.180	15.1	–	3	Egg1956	–	NO, ND	n
05167+4600Aa,Ab	76.2	G5IIIe+G0III	0.285	0.056	5.02	0.95	1	Pbx2000b	Pbx2000b	Y	–
05333+4449	65.2	M2	11.40	0.041	–	–	9	USN1988a	–	NV	–
05544+2017	115.4	G0V	14.12	0.090	–	–	9	Hal2002	Nid2002	Y	–
06003-3102AC	61.0	K6.5V	390.6	3.95	1.78	–	5	Baz1980b	–	NV	nt
06262+1845AB	67.9	K3Vk	600	3.23	0.30	–	5	Hle1994	–	NO	nt
06293-0248AB	242.3	M4.5V	16.12	1.04	0.30	0.51	4	Sgr2000	Sgr2000	Y	n
06451-1643AB	379.2	A1V	50.09	7.50	3.08	–	2	B1960c	A1918b	Y	–
06579-4417AB	124.8	M0.3	298.3	4.396	0.49	–	5	Zir2003	–	NV	n
07100+3832	158.9	M4.5V	0.028	0.011	0.42	0.85	8	Sgr2012	Sgr2012	Y	n
07175-4659AB	68.5	K3V	85.2	1.00	0.43	–	4	Mns2011c	–	NV	n
07346+3153AB	64.1	A2Vm	444.9	6.593	5.49	–	3	Doc1985c	VD	Y	nt
07393+0514AB	284.5	F5IV-V	40.82	4.271	2.03	–	3	Grr2000	Duq1991b, VD	Y	n
07518-1354AB	60.6	G0V	22.70	0.602	1.90	0.97	2	Pbx2000b	Pbx2000b	Y	–
08592+4803A,BC	68.9	A7V	817.9	9.092	3.43	–	5	Hop1973a	–	NO, ND	nt

Notes. See text for the description of the column contents.

Table 2. continued.

WDS	$\varpi$ (mas)	Sp	$P$ (yr)	$a$ (")	$M_{\text{tot}}$ ( $M_{\odot}$ )	$q$	Gr	V.Orb.	S.Orb.	A	Notes
09006+4147AB	62.2	F4V + K0V	21.77	0.633	3.42	0.98	1	New	New	Y	n
09144+5241AB	172.1	M0.0V	975	16.72	0.97	-	4	Chg1972	VD	Y	n
09313-1329AB	99.9	M2V	18.40	0.630	0.74	0.94	3	Sod1999	-	ND	n
09357+3549AB	87.9	G8IIIv	201	3.840	2.06	-	5	Hei1988d	-	NO, NV	n
10454+3831AB	71.9	M2V	160.7	1.791	0.60	-	4	Mnt2000a	-	NV	nt
11182+3132AB	127.0	G0V	59.88	2.536	2.24	1.15	1	Msn1995	Gri1998	Y	nt
11182+3132Aa,Ab	127.0	G0V	1.834	0.054	1.20	0.44	9	Hei1996	Gri1998	Y	nt
11247-6139AB	72.9	K5V+M0Ve	399.4	5.672	2.95	-	4	Sca2002c	-	NV	n
12417-0127AB	85.6	F0V+F0V	169.10	3.639	2.69	-	2	Sca2007c	-	NV	-
13100+1732AB	56.1	F5V+F5V	25.97	0.661	2.43	-	1	Mut2010b	-	ND	n
13169+1701AB	90.3	K2V	770	8.06	1.20	-	4	Hle1994	-	NO	n
13198+4747AB	93.4	K0V	48.91	1.507	1.76	-	2	Msn1999a	-	IC	nt
13328+1649AB	78.4	M2.5V	430	3.17	0.36	-	5	Hei1990d	-	NV	-
13473+1727AB	64.3	F6IV	2000	14.39	2.80	-	5	Hle1994	-	NO, ND	n
13491+2659AB	74.6	K4V+K6V	155.7	2.433	1.43	-	2	Hei1988d	SD	Y	n
13547+1824	87.7	G0V	1.353	0.036	-	-	9	Jnc2005	Jnc2005	Y	n
14035+1047	58.9	G8V	9.897	0.1053	-	-	9	HIP1997d	Nid2002	Y	-
14396-6050AB	754.8	G2V	79.91	17.57	1.98	0.85	2	Pbx2002	Pbx2002	Y	-
14514+1906AB	149.0	G8V	151.6	4.94	1.59	-	2	Sod1999	VD	Y	n
14540+2335AB	98.4	M3V	34.10	0.69	0.30	-	4	Hei1990c	-	NV	-
14575-2125AB	171.2	K4V	2130	32.34	1.49	-	5	Hle1994	-	NO, ND	nt
14575-2125Ba,Bb	168.8	M1.5V	0.846	0.151	1.00	0.73	3	Frv1999	Pbx2000b	Y	t
15038+4739AB	79.9	G0Vnv	209.8	3.666	2.19	-	2	Zir2011	VD	Y	nt
15232+3017AB	56.0	G2V	41.63	0.862	2.11	0.89	1	Mut2010b	VD	Y	-
15527+4227	62.9	F8Ve	0.168	0.001	-	-	9	HIP1997d	-	NO, ND	n
16240+4822Aa,Ab	124.1	M0.3V	3.74	0.237	0.50	-	2	Llo2007	Nid2002	Y	t
16413+3136AB	93.3	G0IV	34.45	1.33	2.44	-	1	Sod1999	new	Y	nt
16555-0820AB	161.4	M3.5Ve	1.717	0.226	1.05	1.61	1	Maz2001	Maz2001	Y	nt
17121+4540AB	167.3	K5V	12.95	0.762	0.56	-	2	Hrt1996a	New	Y	n
17153-2636AB	168.5	K2V	568.9	14.7	1.5	-	4	Irw1996	Irw1996	Y	n
17190-3459AB	146.3	K3V+K5V	42.15	1.81	1.07	-	2	Sod1999	-	NV	-
17191-4638AB	113.6	G8V	693.2	10.45	1.62	-	5	Wie1957	-	NV	n
17304-0104AB	61.2	G9IV-V	46.4	0.98	1.91	0.92	1	Hei1994a	Pbx2000b	Y	n
17349+1234	67.1	A5IV+K2V	8.620	0.427	3.46	0.36	5	Hnk2011	Kam1989	Y	n
17350+6153AB	70.5	G0Va	76.1	1.53	1.77	-	3	Sod1999	Duq1991b, VD	Y	-
17364+6820Aa,Ab	220.8	M3.5V	24.5	0.102	-	-	9	Lip1967	-	NV	nt
17465+2743BC	120.3	M3.5V	43.2	1.360	0.77	-	2	Cou1960b	VD	Y	nt

Table 2. continued.

WDS	$\varpi$ (mas)	Sp	$P$ (yr)	$a$ (")	$M_{\text{tot}}$ ( $M_{\odot}$ )	$q$	Gr	V.Orb.	S.Orb.	A	Notes
18055+0230AB	196.7	K0V	88.37	4.526	1.56	0.87	1	Egn2008	Pbx2000b	Y	-
18070+3034AB	63.9	F7V	56.4	1.00	1.20	-	2	Sod1999	New	Y	nt
18211+7244Aa,Ab	124.1	F7V	0.768	0.124	1.71	0.78	1	CIA2010	Pbx2000b	Y	t
18428+5938AB	280.2	M3.0V	408	13.88	0.73	-	4	Hei1987b	-	ND	n
18570+3254AB	67.2	G0V+K1V	61.41	1.276	1.81	-	2	Mut2010e	Duq1991b,Abt2006	Y	n
19074+3230Ca,Cb	120.2	M3V	5.77	0.288	0.4	0.93	4	Sgr2000	Sgr2000	Y	t
19121+0254AB	97.8	M3.5V	2.466	0.148	0.57	0.51	2	AST1999	AST2001	Y	n
19167-4553AB	62.1	M0Vk	7.70	0.260	1.24	-	3	Sod1999	-	NV	-
19255+0307Aa,Ab	64.4	F0IV	3.426	0.056	-	-	9	HIP1997d	Kam1989	Y	nt
20452-3120BC	93.5	M4Ve	209	3.18	0.90	-	5	Hrt2003	-	ND	t
21000+4004AB	65.4	M3.0V	29.16	0.725	1.60	0.32	4	Doc2010d	Pbx2000b	Y	nt
21069+3845AB	286.8	K5V	678	24.27	1.32	0.62	4	PkO2006b	SD	Y	n
21313-0947AB	117.5	M4.5Ve	1.92	0.141	0.45	0.56	4	Sgr2000	Sgr2000	Y	-
21379+2743Aa,Ab	75.1	M0V	68.0	1.50	-	-	9	Sod1999	-	NV	t
22070+2521	85.3	F5V	0.028	0.010	2.27	0.62	8	Knc2010	Fek1983	Y	-
22234+3228AB	64.5	M0Ve	90.0	1.401	1.27	-	5	USN2002	-	NV	n
22280+5742AB	249.9	M3V+M4V	44.67	2.383	0.45	0.65	2	Hei1986	SD	Y	n
22385-1519AB	293.6	M6V	2.25	0.347	0.33	0.54	2	Sgr2000	Sgr2000	Y	-
23317+1956AB	161.8	M3.5V	359	6.87	0.59	-	5	Hei1984a	-	NO,NV	n
23524+7533AB	91.8	K3V	290	4.14	1.09	-	5	Hle1994	-	NO,NV	nt

**Table 3.** Position of the 51 orbital poles in Galactic coordinates for systems closer than 18 pc.

WDS	Geometrical elements			System coordinates			Parallax (mas)	Pole			Distance (pc)	N	Note	
	$i$ (°)	$\Omega$ (°)	$\omega$ (°)	$\alpha$ (°)	$\delta$ (°)	$\delta$ (°)		$l$ (°)	$b$ (°)	$x$				$y$
00022+2705AB	49.0	290.0	96.0	0.542	27.082	82.2	223.5	63.0	-0.32904	-0.31178	0.89136	12.2	32	-
00057+4549AB	54.9	13.5	267.2	1.418	45.812	88.4	245.5	-9.2	-0.40949	-0.89835	-0.15902	11.3	29	nt
00373-2446AB	78.6	292.0	318.1	9.332	-24.767	64.9	144.2	12.4	-0.79180	0.57162	0.21519	15.4	42	-
00491+5749AB	34.8	278.4	268.6	12.271	57.817	168.0	296.0	39.3	0.33970	-0.69529	0.63339	6.0	12	-
01083+5455Aa,Ab	104.7	224.6	330.0	17.068	54.920	132.4	60.2	36.3	0.40124	0.69932	0.59157	7.6	17	nt
01418+4237AB	105.0	33.0	22.0	25.444	42.614	78.5	214.6	-24.5	-0.74952	-0.51624	-0.41438	12.7	34	n
02171+3413Aa,Ab	163.0	37.0	171.0	34.260	34.225	92.7	161.2	-28.8	-0.82900	0.28284	-0.48246	10.8	28	t
02278+0426AB	73.0	290.1	49.1	36.941	4.432	58.3	138.1	54.2	-0.43560	0.39148	0.81055	17.1	50	n
03121-2859AB	81.0	117.0	43.0	48.018	-28.989	70.9	347.2	-7.8	0.96589	-0.22017	-0.13634	14.1	37	t
05167+4600Aa,Ab	137.2	220.9	269.0	79.172	45.999	76.2	121.1	-6.0	-0.51300	0.85197	-0.10480	13.1	35	-
05544+2017	95.9	126.4	291.5	88.596	20.276	115.4	269.8	-66.5	-0.00114	-0.39882	-0.91703	8.7	25	-
06293-0248AB	51.8	210.7	43.0	97.348	-2.814	242.3	78.1	-20.5	0.19297	0.91631	-0.35091	4.1	7	n
06451-1643AB	136.5	44.6	147.3	101.289	-16.713	379.2	268.0	6.7	-0.03496	-0.99260	0.11628	2.6	2	-
07100+3832	100.4	270.0	32.0	107.508	38.529	159.0	92.6	21.6	-0.04169	0.92898	0.36777	6.3	15	n
07346+3153AB	114.6	41.5	253.3	113.650	31.889	64.1	262.4	35.1	-0.10871	-0.81102	0.57482	15.6	44	nt
07393+0514AB	31.1	277.3	272.2	114.827	5.228	284.6	59.2	5.1	0.51046	0.85536	0.08824	3.5	4	n
07518-1354AB	80.4	102.9	73.1	117.943	-13.897	60.6	329.2	-43.4	0.62419	-0.37154	-0.68727	16.5	49	-
09006+4147AB	133.2	23.8	212.7	135.161	41.783	62.2	255.3	71.0	-0.08263	-0.31472	0.94558	16.1	46	n
09144+5241AB	21.0	173.8	44.0	138.595	52.687	172.1	332.0	-62.2	0.41137	-0.21885	-0.88480	5.8	9	n
11182+3132A	91.0	318.0	144.0	169.546	31.529	127.0	65.6	14.6	0.40030	0.88102	0.25212	7.9	18	nt
11182+3132AB	122.1	101.9	127.9	169.546	31.529	127.0	267.6	27.9	-0.03655	-0.88288	0.46818	7.9	19	nt
13491+2659AB	47.4	335.4	20.0	207.268	26.980	74.6	71.8	-53.5	0.18603	0.56546	-0.80352	13.4	36	n
13547+1824	115.7	75.2	146.3	208.671	18.399	87.8	327.7	12.6	0.82479	-0.52194	0.21748	11.4	30	n
14035+1047	93.5	252.3	9.0	210.885	10.788	58.9	143.9	24.5	-0.73486	0.53655	0.41484	17.0	49	-
14396-6050AB	79.2	204.9	231.7	219.920	-60.835	754.8	210.3	47.8	-0.57995	-0.33945	0.74056	1.3	1	-
14514+1906AB	139.0	347.0	203.0	222.847	19.101	149.0	47.3	23.9	0.62020	0.67219	0.40436	6.7	16	n
14575-2125Ba,Bb	107.6	15.9	307.6	224.358	-21.407	168.8	22.1	-26.5	0.82935	0.33632	-0.44616	5.9	11	t
15038+4739AB	83.6	57.1	39.9	225.949	47.654	80.0	352.0	-8.8	0.97878	-0.13669	-0.15263	12.5	33	nt
15232+3017AB	58.1	22.8	219.9	230.801	30.288	56.0	12.1	-62.0	0.45854	0.09852	-0.88320	17.9	51	-
16240+4822Aa,Ab	154.0	278.5	68.7	246.035	48.354	124.1	105.1	32.5	-0.22040	0.81412	0.53725	8.1	20	t
16413+3136AB	132.0	235.2	297.0	250.323	31.602	93.3	124.7	56.6	-0.31360	0.45246	0.83483	10.7	27	nt
16555-0820AB	163.1	163.2	115.6	253.872	-8.334	161.4	355.9	31.2	0.85285	-0.06111	0.51857	6.2	14	nt

**Notes.**  $\omega$  is the position of the longitude of periastron of the visual orbit (B with respect to A; it differs by 180° from the value for the spectroscopic orbit of A with respect to the centre of mass).  $N$  ranks the systems in order of increasing distance.

Table 3. continued.

WDS	Geometrical elements			System coordinates		Parallax		Pole			Distance (pc)	N	Note	
	$i$ (°)	$\Omega$ (°)	$\omega$ (°)	$\alpha$ (°)	$\delta$ (°)	(mas)	$l$ (°)	$b$ (°)	$x$	$y$				$z$
17121+4540AB	149.1	160.0	99.0	258.032	45.670	167.3	45.2	62.2	0.32882	0.33098	0.88449	6.0	13	n
17153+2636AB	99.6	255.1	276.4	258.839	-26.600	167.1	81.6	50.3	0.09338	0.63199	0.76933	6.0	10	n
17304+0104AB	99.1	332.3	148.1	262.599	-1.063	61.2	91.6	-28.1	-0.02432	0.88198	-0.47066	16.3	47	n
17349+1234	125.0	232.0	162.0	263.733	12.561	67.1	92.4	62.9	-0.01906	0.45448	0.89055	14.9	39	n
17350+6153AB	104.0	151.0	307.0	263.747	61.876	70.5	329.1	59.8	0.43199	-0.25880	0.86395	14.2	38	-
17465+2743BC	66.2	240.7	354.0	266.605	27.717	120.3	189.4	26.0	-0.88700	-0.14733	0.43764	8.3	22	nt
18055+0230AB	121.1	301.7	13.4	271.363	2.502	196.7	88.6	2.0	0.02510	0.99905	0.03564	5.1	8	-
18070+3034AB	39.8	227.2	290.7	271.757	30.562	64.0	219.0	13.4	-0.75569	-0.61253	0.23180	15.6	45	nt
18211+7244Aa,Ab	74.4	50.3	299.3	275.260	72.734	124.1	18.3	-43.3	0.69070	0.22838	-0.68613	8.1	21	t
18570+3254AB	114.2	48.8	281.7	284.256	32.902	67.2	30.2	-45.4	0.60754	0.35323	-0.71142	14.9	40	n
19074+3230Ca,Cb	77.3	265.1	150.9	286.928	32.544	120.2	174.1	26.0	-0.89409	0.09184	0.43837	8.3	23	t
19121+0254AB	131.5	358.8	206.5	288.056	2.888	97.8	67.8	-44.0	0.27214	0.66594	-0.69460	10.2	26	n
19255+0307Aa,Ab	150.0	337.0	191.0	291.374	3.115	64.4	64.7	-24.0	0.39046	0.82565	-0.40725	15.5	43	nt
21000+4004AB	53.0	96.8	156.1	315.020	40.071	65.4	308.7	-23.9	0.57205	-0.71280	-0.40579	15.3	41	nt
21069+3845AB	51.0	178.0	149.0	316.725	38.749	286.8	305.8	38.3	0.45917	-0.63651	0.61969	3.5	5	n
21313-0947AB	46.0	144.4	188.7	322.827	-9.791	120.5	286.5	44.2	0.20316	-0.68798	0.69671	8.3	24	-
22070+2521	95.8	356.3	92.8	331.752	25.345	85.3	182.8	-35.3	-0.81561	-0.03923	-0.57727	11.7	31	-
22280+5742AB	167.2	334.5	31.0	336.998	57.696	249.9	117.4	-1.3	-0.46041	0.88741	-0.02292	4.0	6	n
22385-1519AB	112.6	161.2	338.7	339.64	-15.299	294.3	6.0	1.8	0.99401	0.10469	0.03149	3.4	3	-

## Appendix A: Notes on individual systems and new orbits

**WDS 00057+4549AB.** The Sixth Catalog of Orbits of Visual Binary Stars lists two orbits for the AB pair of that system (separated by about  $6''$ ): one with a period of 1550 yr (Popovic & Pavlovic 1996) and another with a period of 509 yr (Kiyaveva et al. 2001), indicating that the solution is not yet well constrained. Radial velocities obtained by CORAVEL and by Tokovinin & Smekhov (2002), as listed in Table A.4 and displayed in Fig. A.1, correspond to a radial velocity difference  $V_B - V_A$  slightly decreasing from  $-2.7 \text{ km s}^{-1}$  in 1980 to  $-3.8 \text{ km s}^{-1}$  in 1996. The value  $-3.0 \text{ km s}^{-1}$  has been used by Kiyaveva et al. (2001) to determine unambiguously the ascending node. This result is confirmed thanks to the precise radial-velocity measurements of Marcy (2013, priv. comm.) that show a linear variation for  $V_B - V_A$  amounting to  $-6.4 \text{ m s}^{-1} \text{ yr}^{-1}$  from 2000 to 2010, while a value of  $-11.5 \text{ m s}^{-1} \text{ yr}^{-1}$  is calculated from the visual orbit. Thus we have computed the position of the orbital pole but it is not expected to be precise.

Kiyaveva et al. (2001) also suggested that ADS 48 ABF is a hierarchical triple system whose orbits (AB) and (AB-F) are not coplanar. This hypothesis was contradicted by Cvetković et al. (2012), who concluded that the F component has a common proper motion with the AB pair, but that it is not bound by gravity.

**WDS 00184+4401AB.** Indeterminate visual orbit.

**WDS 00321+6715Aa,Ab and AB.** The preliminary visual orbits of this triple hierarchical system were computed by Docobo et al. (2008). No radial velocity measurements are available to resolve the ambiguity of the ascending node.

**WDS 01083+5455Aa,Ab.** Drummond et al. (1995) obtained the first relative astrometric orbit for that system from their direct detection of the faint B component. Combining that orbit with earlier photocentric positions (Lippincott 1981; Russell & Gatewood 1984), masses could be derived:  $M_A = 0.74 \pm 0.06 M_\odot$  and  $M_B = 0.17 \pm 0.01 M_\odot$ .

Duquennoy & Mayor (1991) derived a preliminary spectroscopic orbit, and Abt & Willmarth (2006) obtained thereafter more radial velocities; however, Abt & Willmarth (2006) did not attempt to compute a combined orbit, and merged the orbital elements of Duquennoy & Mayor (1991) and Drummond et al. (1995). Because this is not fully satisfactory and is prone to confusion (as further discussed below), especially regarding the ambiguity on  $\omega$ , we decided to compute a new combined orbit (Fig. A.2), using data of Duquennoy & Mayor (1991) as well as more recent unpublished CORAVEL data (Table A.5), plus velocities reported by Abt & Willmarth (2006). The astrometric positions of B relative to A taken from the WDS database at USNO were used as well. As shown in Table A.2, the value of  $\omega$  for the astrometric orbit of B around A is  $329.4^\circ \pm 3.8^\circ$  (thus a change of  $180^\circ$  from the relative orbit of Drummond et al. 1995; their Table 9), and we stress that the value ( $332.7^\circ \pm 3.1^\circ$ ) listed by Abt & Willmarth (2006) for the spectroscopic orbit (of A around the centre of mass of the system) is incorrect, as it should differ by  $180^\circ$  from the astrometric value, confirming the suspected confusion. It is in fact just the value reported by Drummond et al. (1995), which should not have been copied without change! Instead, the value ( $147.9^\circ \pm 4.9^\circ$ ) of Duquennoy & Mayor (1991) for the spectroscopic orbit is correct.

**WDS 01398-5612AB.** Indeterminate visual orbit. In the absence of recent radial-velocity measurements it is not possible to lift the ambiguity on the position of the ascending node.

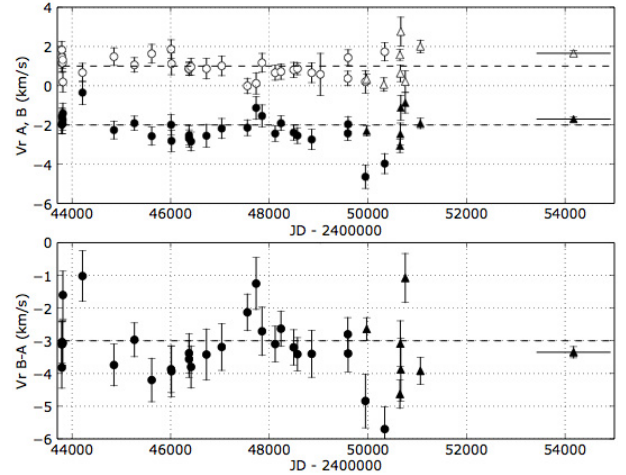


**Fig. A.1.** *Top panel:* radial velocities for the two components of the pair HIP 473 AB = WDS 00057+4549AB. Dots refer to CORAVEL velocities and triangles to velocities from Tokovinin & Smekhov (2002) or Chubak et al. (2012) for the last point, with the time spanned by the measurements represented by the horizontal bar. Open symbols refer to component A and filled symbols to component B. The parallel dashed lines are just a guide to the eye. *Bottom panel:* radial-velocity difference B-A, with their errors taken as the root-mean-square of the errors on A and B.

**WDS 01418+4237AB.** Spectroscopic orbits were published by Duquennoy & Mayor (1991) and Abt & Willmarth (2006). The present orbit (Table A.2) improves upon those, as it includes several unpublished CORAVEL velocities given in Table A.6. Lippincott et al. (1983) and Söderhjelm (1999) published astrometric orbits. Here, we obtained a combined astrometric/spectroscopic solution by considering the astrometric measurements from the Fourth Catalogue of Interferometric Measurements of Binary Stars<sup>12</sup>. This solution agree well with the existing solutions quoted above.

**WDS 01425+2016AB.** This system was announced as an astrometric binary with a period of 0.567 yr by the *Double and Multiple Star Annex* (DMSA) of the HIPPARCOS Catalogue (ESA 1997). However, reprocessing the HIPPARCOS data along the method outlined by Pourbaix (2000) for a combined solution including the CORAVEL velocities does not allow us to confirm the HIPPARCOS DMSA/O solution. This system was therefore dropped from our final list.

**WDS 02278+0426AB.** The most recent and thorough analysis of that system was presented by Andrade (2007), including a revised visual orbit. CORAVEL data (Table A.7) make it possible now to compute a combined SB2/astrometric orbit, which thus gives access for the first time to the masses of the system components. The combined orbital elements and other physical parameters of the system (such as orbital parallax and component masses) are listed in Table A.3, which identifies the components as 1 and 2 rather than A and B. It must be stressed that there is no easy way to identify for sure the spectroscopic component 1 with either visual component A or B, since both components fall in the spectrograph slit and are of almost equal brightness: HIPPARCOS gives  $m_{\text{Hp},A} = 9.45$  and  $m_{\text{Hp},B} = 9.63$ . An indirect way to identify components A and B is by noting that in Table A.3, the velocity semi-amplitude  $K_2$  is higher than  $K_1$ , hence  $M_2$  is smaller than  $M_1$ . Since both components lie

<sup>12</sup> Available from

<http://www.usno.navy.mil/USNO/astrometry/optical-IR-prod/wds/int4>

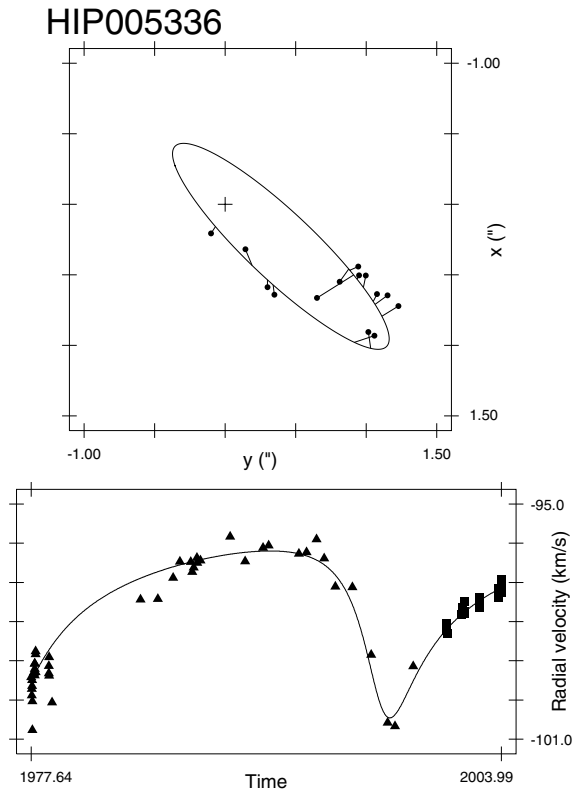


**Fig. A.2.** Combined astrometric (*upper panel*) and spectroscopic (*lower panel*) orbits for WDS 01083+5455Aa,Ab = HIP 5336 = HD 6582 =  $\mu$  Cas. The solid line in the lower panel corresponds to the predicted velocity curve for A. Triangles are CORAVEL measurements, squares are measurements from [Abt & Willmarth \(2006\)](#). Individual measurements for the visual orbit were taken from the WDS database.

on the main sequence, component 2 should thus be less luminous than component 1, hence component 2 should be identified with B. It is possible to check quantitatively this assumption by using the mass-luminosity relationship provided by [Kroupa et al. \(1993\)](#), namely  $M_{V,1} = 5.4$  for  $M_1 = 0.95 M_{\odot}$  and  $M_{V,2} = 6.2$  for  $M_2 = 0.85 M_{\odot}$ , or  $M_{V,2} - M_{V,1} = 0.8$ , somewhat larger than the observed  $m_{HP,B} - m_{HP,A} = 0.18$ , but certainly consistent with the error bars on  $M_{1,2}$ . Although [Andrade \(2007\)](#) classified HD 15285 A as K7V based on several spectral features, among which the presence of weak TiO bands, its inferred mass of  $0.95 M_{\odot}$  is more typical of a G5V type, while the mass of component B would flag it as K0V ([Cox 2000](#)).

These masses were derived from the orbital parallax of  $52 \pm 2$  mas, to be compared with the HIPPARCOS value of  $60.2 \pm 1.7$  mas ([ESA 1997](#)) or  $58.3 \pm 1.1$  mas ([van Leeuwen 2007](#)), which yield total masses of 1.16 and 1.28  $M_{\odot}$ , respectively, to be compared with 1.8  $M_{\odot}$  for the orbital parallax. From the fractional mass  $M_2/(M_1 + M_2) = 0.47$  (Table A.3), one obtains,  $(M_1, M_2) = (0.62, 0.54)$  and  $(0.68, 0.60) M_{\odot}$ . These values agree much better with a K7V spectral type for component A.

**WDS02361+0653A.** The 22 CORAVEL measurements available for component A (spanning 6837 d) yield a standard deviation of  $0.29 \text{ km s}^{-1}$ , identical to the average error on a single measurement. The constancy of the radial velocity was confirmed by [Chubak et al. \(2012\)](#), who obtained 62 measurements spanning 1299 d, with a standard deviation of  $0.142 \text{ km s}^{-1}$ . Hence, radial velocities cannot be used to lift the ambiguity on the orbital orientation.

**WDS 02442+4914AB.** Indeterminate visual orbit and roughly constant radial velocity between 1900 and 1990.

**WDS 03575-0110AB.** Indeterminate visual orbit and almost constant radial velocity between 1984 and 1993.

**WDS 04153-0739BC.** In the triple system STF 518 A-BC, B is the white dwarf omi Eri B and C the flare star DY Eri.

**WDS 04312+5858Aa,Ab.** Triple system, with the A component being an astrometric binary in the visual binary STI 2051 AB.

**WDS 05074+1839AB.** Visual orbit highly conjectural and radial velocity from [Duquennoy & Mayor \(1991\)](#) is constant.

**WDS 06003-3102AC.** A quadruple system ([Tokovinin et al. 2005](#)): HU 1399 AB ( $P = 67.7 \text{ yr}$ ,  $a = 0.912''$ ), HJ 3823 AC ( $P = 390.6 \text{ yr}$ ,  $a = 3.95''$  by Baize 1980, not confirmed by Tokovinin et al. 2005), TOK 9 C,CE ( $P = 23.7 \text{ yr}$ ,  $a = 0.12''$ ). A, B and C, CE are coplanar ([Tokovinin et al. 2005](#)).

**WDS 06262+1845AB.** Triple system, with A known as SB2 with  $P = 6.99 \text{ d}$  ([Griffin & Emerson 1975](#)).

**WDS 06293-0248AB.** Solution for the SB2 orbit includes masses and orbital parallax ([Ségransan et al. 2000](#)). Although not clearly stated, the orbital elements listed by [Ségransan et al. \(2000\)](#) correspond to the spectroscopic orbit (hence  $\omega$  and  $\Omega$  listed in our Table 3 differ by  $180^\circ$  from theirs).

**WDS 06579-4417AB.** Indeterminate visual orbit.

**WDS 07100+3832.** The spectro-visual orbit of this system was only recently computed by [Barry et al. \(2012\)](#).

**WDS 07175-4659AB.** The visual orbit is still very uncertain. The total mass of the system is abnormally low given the spectral type.

**WDS 07346+3153AB.** A difficult system since both A and B are spectroscopic binaries ([Vinter Hansen et al. 1940](#)), with  $P = 9.21 \text{ d}$  and  $P = 2.93 \text{ d}$ , respectively. [Batten \(1967\)](#) has lifted the ambiguity on the ascending node for that system, and we used the orbital elements of the 6th Catalogue of Visual Binary Orbits to compute the position of the pole, agreeing with that of [Batten \(1967\)](#), allowing for the fact that our poles follow the right-hand rule, opposite to that of Batten.

**WDS07393+0514AB.** The pole ambiguity was lifted from the radial-velocity drift present in the [Duquennoy et al. \(1991\)](#) data.

**WDS 08592+4803A,BC.** Indeterminate visual orbit. It might be a quadruple system, since Aa seems to be a SB1 system with a period  $P \sim 11 \text{ yr}$  ([Abt 1965](#)) although the spectroscopic orbit is not of an excellent quality.

**WDS 09006+4147AB.** The period of 21.05 yr for that visual binary is well established ([Muterspaugh et al. 2010a](#)). Based on an older (albeit similar) value of the visual period from [Heintz \(1967\)](#), [Abt & Levy \(1976\)](#) proposed a spectroscopic orbit based on Heintz' visual elements plus approximate values for the systemic velocity and the semi-amplitude, which could account for Abt & Levy's own velocity measurements and older ones from [Underhill \(1963\)](#). Although it is rather uncertain, this orbit is still the one quoted by the SB9 catalogue ([Pourbaix et al. 2004](#)). The spectroscopic orbit is difficult to derive because (i) the components are not separated widely enough on the sky to record their spectra separately; (ii) the velocity semi-amplitude is small; and (iii) component A appears to rotate relatively fast. Therefore, the available unpublished CORAVEL measurements appear useless, since the two components appear hopelessly blended in the cross-correlation function. More recent HERMES/Mercator spectra ([Raskin et al. 2011](#)) have a resolution high enough to allow a comfortable double-Gaussian fit of the cross-correlation function (CCF; Fig. A.5). Although such a fit has not necessarily a unique solution, we found it re-assuring that the CCFs for all seven available dates (Table A.1) are well fitted with Gaussians having the same properties: height  $\sim 0.08$  and  $\sigma = 14 \text{ km s}^{-1}$

**Table A.1.** HERMES and CORAVEL radial velocities for components of some visual binaries lacking velocities so far.

JD-2 400 000	$V_r(A)$	$V_r(B)$	HER/COR	Note
WDS 09006+4147AB				
55 520.795	$29.06 \pm 0.09$	$22.06 \pm 0.08$	H	a
55 521.640	$29.03 \pm 0.10$	$21.93 \pm 0.09$	H	–
55 579.783	$29.44 \pm 0.09$	$21.83 \pm 0.08$	H	–
55 589.620	$29.53 \pm 0.09$	$21.68 \pm 0.08$	H	–
55 647.599	$29.64 \pm 0.08$	$21.45 \pm 0.07$	H	–
56 046.402	$31.11 \pm 0.09$	$19.92 \pm 0.05$	H	–
56 244.717	$31.54 \pm 0.13$	$19.48 \pm 0.07$	H	–
WDS 09144+5241A				
56 039.412	$10.620 \pm 0.002$	–	H	–
WDS 09144+5241B				
56 039.418	–	$11.848 \pm 0.002$	H	–
WDS 10454+3831AB				
56 040.468	$-3.380 \pm 0.003$	–	H	–
56 040.485	–	$-3.175 \pm 0.005$	H	b
WDS 13491+2659AB				
45 441.525	$-20.32 \pm 0.32$	–	C	–
45 475.401	$-19.29 \pm 0.45$	$-22.70 \pm 0.42$	C	–
45 789.537	$-20.27 \pm 0.33$	$-23.18 \pm 0.37$	C	–
46 214.395	$-20.06 \pm 0.32$	$-23.95 \pm 0.35$	C	–
46 562.422	$-20.48 \pm 0.31$	$-23.80 \pm 0.37$	C	–
51 018.433	$-20.27 \pm 0.44$	$-23.01 \pm 0.46$	C	–
WDS 17153-2636A				
56 038.716	$0.532 \pm 0.002$	–	H	–
WDS 17153-2636B				
56 038.719	–	$0.246 \pm 0.001$	H	–
WDS 17364+6820Aa,Ab				
55 6038.682	$-30.0 \pm 0.3$	$-27.0 \pm 0.5$	H	c
WDS 18428+5938AB				
55 655.719	$-1.061 \pm 0.006$	–	H	–
55 660.748	$-1.048 \pm 0.005$	–	H	–
56 037.736	$-1.074 \pm 0.005$	–	H	–
56 038.695	$-1.088 \pm 0.005$	–	H	–
56 038.699	–	$0.779 \pm 0.006$	H	–
WDS 19255+0307Aa,Ab				
55 657.742	$-28.68 \pm 0.26$	$-37.70 \pm 0.09$	H	

**Notes.** The quoted error corresponds to the fitting error, but does not account for the pressure-driven zero-point shift, which can amount up to  $200 \text{ m s}^{-1}$  for HERMES velocities (Raskin et al. 2011). a: Component A ( $V = 4.2$ ), of spectral type F4V, is a fast rotator. It has the largest peak on the HERMES cross-correlation function (Fig. A.5). For details see note in Appendix A; b: barely separable; c: “blind” assignment based on the depth of the cross-correlation peak: component A is assumed to have the deeper peak.

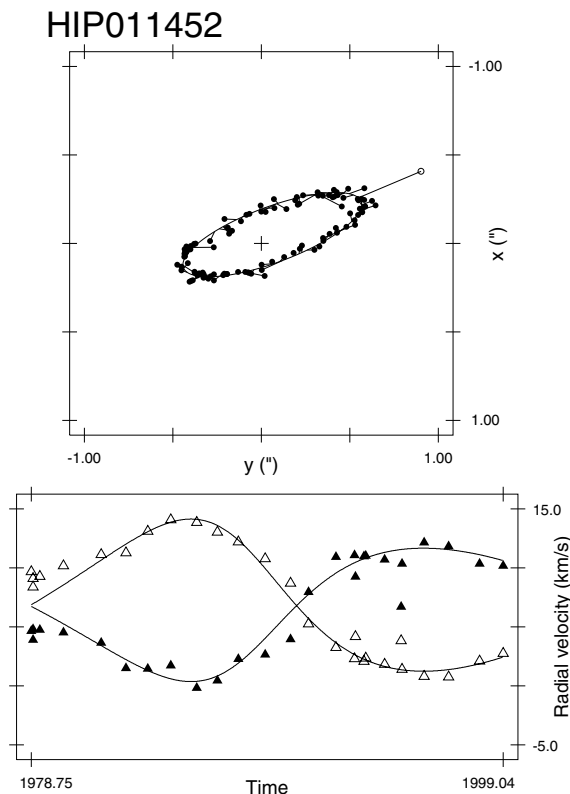


**Fig. A.3.** Combined astrometric (*upper panel*) and spectroscopic (*lower panel*) orbits for WDS 02278+0426AB. In the *lower panel*, filled and open triangles correspond to CORAVEL velocities for components 1 and 2, respectively. Individual measurements for the visual orbit were taken from the WDS database at USNO.

for the F4V component A ( $V = 4.2$ ), and height  $\sim 0.04$  and  $\sigma = 4 \text{ km s}^{-1}$  for the K0V component B ( $V = 6.5$ ). It thus appears that component A is a relatively fast rotator. The assignment of either of the two CCF peaks to component A thus relies on the assumption that component A, being of spectral type F4V, should correspond to the deepest peak when computed with a F0V template.

The validity of our double-Gaussian fits, and of the resulting orbital elements listed in Table A.3, may be assessed a posteriori by the comparison of the orbital parallax ( $53.8 \pm 1.0 \text{ mas}$ ) with the HIPPARCOS parallax ( $60.9 \pm 1.3 \text{ mas}$ ; ESA 1997). The discrepancy probably comes from the fact that the limited phase coverage for the radial velocities does not yet impose strong enough constraints on the velocity semi-amplitudes (Fig. A.4). The astrometrically derived masses ( $M_A = 1.37 M_\odot$ ,  $M_B = 1.04 M_\odot$ ), in relatively good agreement with the spectral types; Martin & Mignard 1998; Söderhjelm 1999) are different from the types derived from our combined orbit ( $M_A = 1.73 M_\odot$ ,  $M_B = 1.69 M_\odot$ ), which also hints at inaccurate velocity semi-amplitudes.

**WDS 09144+5241AB.** For this long-period binary, the determination of the orbital pole is based on the agreement between the variation of the radial velocities  $V_A$  and  $V_B$  measured between 1910 and 1997 and the value predicted using the elements of the visual orbit. This result is confirmed by the value of the measurement of  $(V_B - V_A)$  performed with the HERMES spectrograph in 2012 (see Table A.1).

**WDS 09313-1329AB.** Mass-ratio derived from the astrometry (Söderhjelm 1999). Two HERMES radial-velocity measurements obtained one year apart neither showed any significant

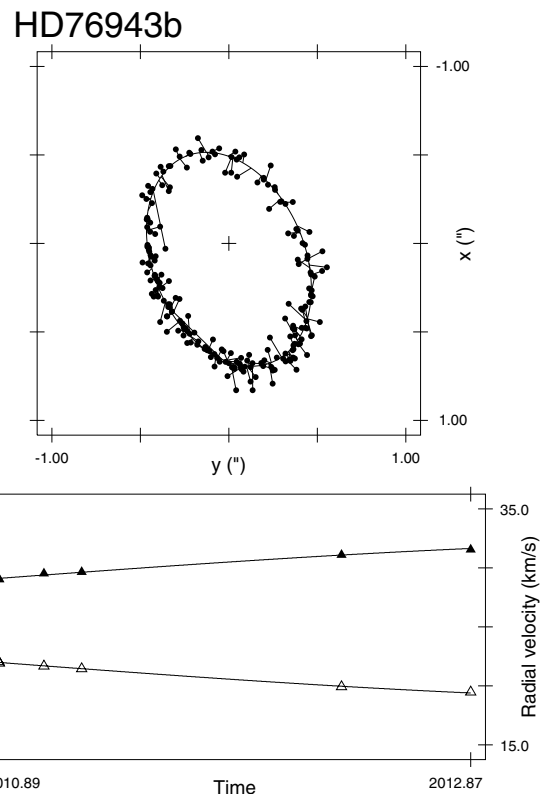


**Fig. A.4.** Combined astrometric (*upper panel*) and spectroscopic (*lower panel*) orbits for WDS 09006+4147AB. Filled triangles in the *lower panel* refer to component A. Individual measurements for the visual orbit were taken from the WDS database.

drift ( $V_r = 7.93 \text{ km s}^{-1}$  on JD = 2455 657.5 and  $V_r = 7.89 \text{ km s}^{-1}$  on JD = 2456 038.4), nor any line doubling, as would be expected for a system consisting of two components only 0.6 arcsec apart.

**WDS 09357+3549AB.** Indeterminate visual orbit.

**WDS 10454+3831AB.** Triple system, Aa being the speckle binary CHR 191. A value of  $(V_B - V_A)$  obtained with the HERMES spectrograph in 2012 is listed in Table A.1.

**WDS 11182+3132AB.** Quadruple system, A and B are both SB1 with  $P = 670.24 \text{ d}$  and  $P = 3.98 \text{ d}$  respectively (Griffin 1998).

**WDS 11247-6139AB.** Abnormally high total mass, inconsistent with the spectral types.

**WDS 13100+1732AB.** Spectral types and masses of components from ten Brummelaar et al. (2000).

**WDS 13198+4747AB.** Triple system (Aa = CHR 193; Beuzit et al. 2004). CORAVEL sees this star as SB3, but no satisfactory attribution of the various peaks to the corresponding components could be made, making it very difficult to isolate the trend of  $V_r(A)$ .

**WDS 13473+1727AB.** Indeterminate orbit. The component  $\tau \text{ BooAb}$  is a star with planet.

**WDS 13491+2659AB.** The pole ambiguity was lifted from unpublished CORAVEL velocities yielding the sign of  $V_r(B) - V_r(A)$  ( $= -3.3 \text{ km s}^{-1}$ ) during the observation span 1983–1988 (Table A.1).

**WDS 13547+1824.** Jancart et al. (2005) obtained a combined spectroscopic/astrometric orbit based on HIPPARCOS data and the spectroscopic orbit of Bertiau (1957). The value of  $\omega$  from Jancart et al. (2005) has been adopted in Table 3.

**WDS 14514+1906AB.** The visual orbital period is 151 yr (Söderhjelm 1999), so that no strong trend must be expected

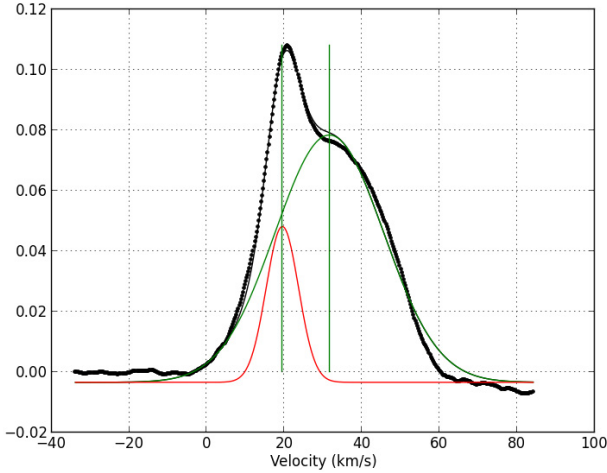


**Fig. A.5.** Cross-correlation function of the spectrum of WDS 09006+4147AB (=HD 76943) obtained with the HERMES/Mercator spectrograph (Raskin et al. 2011) on HJD 2456 244.717 (November 13, 2012), correlated with a FOV template. Both components (separated by  $0.5''$  on the sky) enter the fiber ( $2.5''$  on the sky). Component A corresponds to the wide peak centred at  $31.5 \text{ km s}^{-1}$ .

from the radial velocities over three decades. CORAVEL observations (Duquennoy et al. 1991) exhibit a weak upward trend between 1977 ( $1 \text{ km s}^{-1}$ ) and 1991 ( $1.4 \text{ km s}^{-1}$ ), which is however not significant based on the average measurement uncertainty of  $0.34 \text{ km s}^{-1}$ . Later measurements by Abt & Willmarth (2006) seem to confirm that trend, but the trend is made fragile by a possible zero-point offset between the two data sets. Nevertheless, the pole quoted in Table 3 is based on the assumption that the radial-velocity trend is real, which then implies that the node given in the 6th USNO Catalogue is the correct one.

*WDS 14575-2125AB.* Indeterminate visual orbit.

*WDS 15038+4739AB.* Triple star: Bb = eclipsing SB2 with  $P = 0.27 \text{ d}$  (Lu et al. 2001).

*WDS 15527+4227.* The HIPPARCOS Double and Multiple Star Annex (DMSA; ESA 1997) claims HIP 77760 to be an astrometric binary with an orbital period of 0.14 yr and an inclination of  $131.68^\circ$ . These values seem, however, incompatible with the absence of (CORAVEL) radial-velocity variations (33 measurements with a standard deviation of  $0.413 \text{ km s}^{-1}$ , to be compared with the average instrumental error of  $0.380 \text{ km s}^{-1}$ ).

*WDS 16413+3136AB.* There are many visual orbits available for that system, the most recent ones by Baize (1976) and Söderhjelm (1999). Scarfe et al. (1983) already computed an orbit combining visual data and a collection of Coudé radial velocities. Unpublished CORAVEL velocities given in Table A.8 nicely complement Scarfe's velocities, yielding a somewhat more accurate orbit as listed in Table A.2. A third component has been detected by IR speckle interferometry (McCarthy 1983).

*WDS 16555-0820AB.* A triple system composed of M dwarfs, in which all three stars are visible in the spectra. Spectroscopic orbits are available for the inner (Ba-b) and outer pairs (A-Bab), both as SB2 (Ségransan et al. 2000). The two orbits are probably coplanar (Mazeh et al. 2001). The whole system is probably septuple.

*WDS 17121+4540AB.* A visual orbit for that system was obtained by Hartkopf et al. (1996). The available CORAVEL velocities shown in Table A.9 make it possible to derive a combined orbit for the first time. Visual observations are from the CHARA database. The new combined orbit is presented in Fig. A.7.

**Table A.2.** New combined astrometric-spectroscopic orbits computed from CORAVEL and/or HERMES velocities.

WDS	$P$ (yr)	$a$ (")	$i$ ( $^\circ$ )	$e$	$\omega_B$ ( $^\circ$ )	$\Omega$ ( $^\circ$ )	$T_0$ (yr)	$V_0$ ( $\text{km s}^{-1}$ )	$K_A$ ( $\text{km s}^{-1}$ )
01083+5455Aa,Ab	$21.40 \pm 0.11$	$1.07 \pm 0.04$	$104.7 \pm 1.9$	$0.53 \pm 0.02$	$330.0 \pm 3.4$	$224.6 \pm 2.0$	$1975.9 \pm 0.1$	$-97.35 \pm 0.04$	$2.13 \pm 0.11$
01418+4237AB	$19.73 \pm 0.09$	$0.61 \pm 0.03$	$99.4 \pm 1.5$	$0.43 \pm 0.02$	$223.4 \pm 2.3$	$30.2 \pm 1.7$	$1997.0 \pm 0.1$	$3.31 \pm 0.03$	$2.93 \pm 0.07$
16413+3136AB	$34.447 \pm 0.004$	$1.333 \pm 0.004$	$132.0 \pm 0.2$	$0.452 \pm 0.001$	$297.0 \pm 0.2$	$235.2 \pm 0.2$	$1933.26 \pm 0.009$	$-70.441 \pm 0.008$	$4.01 \pm 0.01$
17121+4540AB	$12.85 \pm 0.05$	$0.88 \pm 0.02$	$134.5 \pm 1.9$	$0.80 \pm 0.01$	$99.9 \pm 1.8$	$165.6 \pm 2.5$	$1990.84 \pm 0.03$	$-30.45 \pm 0.05$	$1.8 \pm 0.1$
18070+3034AB	$56.37 \pm 0.06$	$1.07 \pm 0.02$	$39.8 \pm 1.6$	$0.772 \pm 0.004$	$290.7 \pm 1.0$	$227.2 \pm 1.3$	$1997.72 \pm 0.03$	$0.267 \pm 0.027$	$3.23 \pm 0.03$

**Notes.** The value of  $\omega$  given in the present table corresponds to that of the visual orbit of B around A (it thus differs by  $180^\circ$  from that of A around the centre of mass of the system, obtained for purely spectroscopic binaries).

## HIP081693

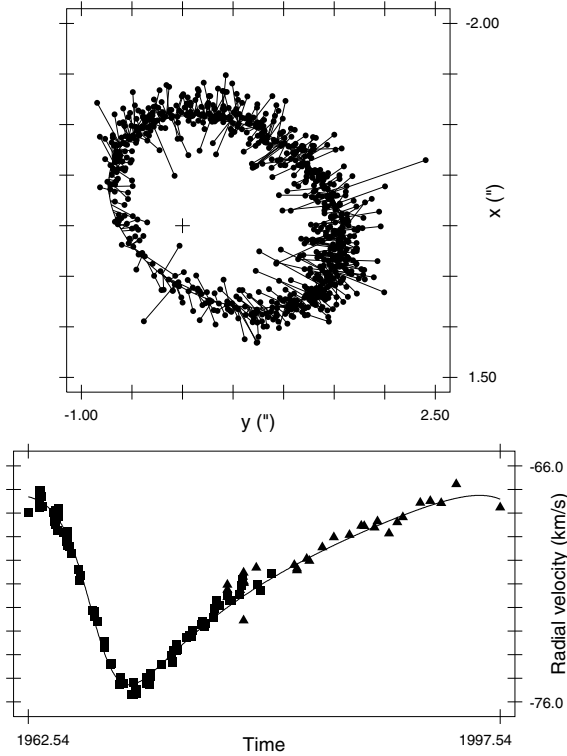


**Fig. A.6.** Combined astrometric (*upper panel*) and spectroscopic (*lower panel*) orbits for WDS 16413+3136AB. The solid line in the lower panel corresponds to the predicted velocity curve for A. Individual measurements for the visual orbit were taken from the WDS database at USNO.

## HIP084140

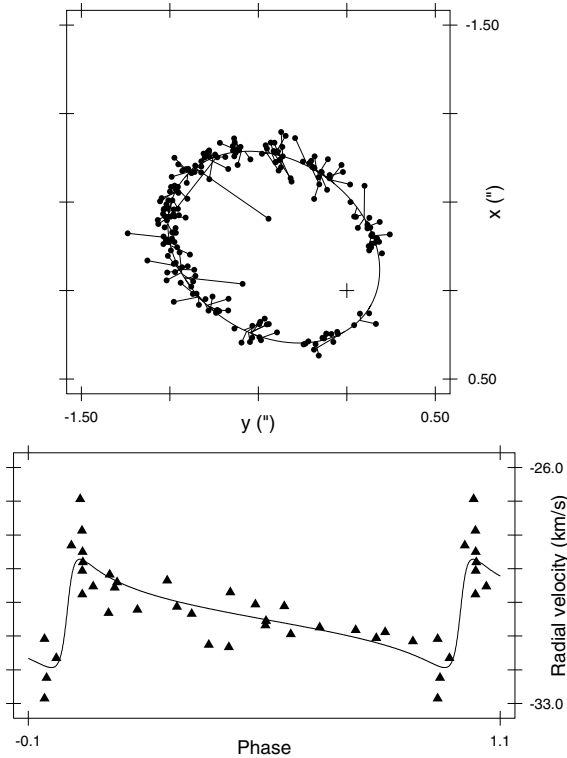


**Fig. A.7.** Combined astrometric (*upper panel*) and spectroscopic (*lower panel*) orbit for WDS 17121+4540AB. The solid line in the lower panel corresponds to the predicted velocity curve for A. Individual measurements for the visual orbit were taken from the WDS database at USNO.

**Table A.3.** New combined astrometric-spectroscopic orbits (2 observable spectra) computed from CORAVEL or HERMES velocities.

WDS	02278+0426AB	09006+4147AB
$P$ (yr)	$25.14 \pm 0.04$	$21.78 \pm 0.02$
$a$ (")	$0.5429 \pm 5.2e-03$	$0.633 \pm 0.004$
$a$ (AU)	$10.390 \pm 0.086$	$11.76 \pm 0.04$
$i$ ( $^\circ$ )	$73.0 \pm 0.7$	$133.2 \pm 0.6$
$\omega_2$ around 1 ( $^\circ$ )	$49.1 \pm 2.6$	$212.7 \pm 1.9$
$\Omega$ ( $^\circ$ )	$290.1 \pm 1.0$	$23.8 \pm 0.8$
$e$	$0.21 \pm 0.01$	$0.154 \pm 0.004$
$T_0$ (Besselian year)	$1962.8 \pm 0.2$	$1972.0 \pm 0.1$
$V_0$ (km s $^{-1}$ )	$6.80 \pm 0.15$	$25.6 \pm 0.1$
$\varpi_{\text{dyn}}$ (")	$0.052 \pm 0.002$	$0.054 \pm 0.001$
$M_1$ ( $M_\odot$ ) <sup>a</sup>	$0.95 \pm 0.10$	1.73:
$M_2$ ( $M_\odot$ )	$0.85 \pm 0.10$	1.69:
$M_2/(M_1 + M_2)$	$0.47 \pm 0.02$	0.5
$K_1$ (km s $^{-1}$ )	$5.6 \pm 0.3^a$	$5.9 \pm 0.2$
$K_2$ (km s $^{-1}$ )	$6.4 \pm 0.3$	$6.0 \pm 0.1$

**Notes.** The value of  $\omega$  given in the present table corresponds to that of the visual orbit of B around A (it thus differs by  $180^\circ$  from that of A around the centre of mass of the system, obtained for purely spectroscopic binaries).  $\varpi_{\text{dyn}}$  is the orbital parallax, which is obtained from the ratio  $a$  (") /  $a$  (AU). <sup>(a)</sup> Most likely, spectroscopic component 1 is WDS 02278+0426 A (see text for details).

**WDS 17153-2636AB.** Irwin et al. (1996) derived precise B-A radial velocities (except for an acceleration component that they were unable to explain). Velocity measurements of  $V_r(A)$  and  $V_r(B)$  were obtained in 2012 by the HERMES spectrograph (Table A.1).

**WDS 17191-4638AB.** Indeterminate visual orbit.

**WDS 17304-0104AB.** A combined astrometric/spectroscopic solution has been computed by Pourbaix (2000) and has been used to compute the position of the orbital pole.

**WDS 17349+1234.** Spectral types from Gatewood (2005). Kamper et al. (1989) performed a combined spectroscopic/astrometric analysis of this system, and their orbit has been recently updated by Hinkley et al. (2011), from whom we adopted the orbital elements without requiring any change to comply with our conventions.

**WDS 17364+6820Aa,Ab.** Velocity measurements of  $V_r(A)$  and  $V_r(B)$  obtained in 2012 by the HERMES spectrograph are listed in Table A.1.

**WDS 17465+2743BC.** HD 161797 ( $\mu$  Her) is a quadruple system (Raghavan et al. 2010). The components of the wide pair STF 2220 AB ( $35''$ ) have common proper motion. The component A is an astrometric binary (period of 65 years, Heintz 1994). The components B and C form the visual binary AC 7 for which the orbital pole ambiguity has been lifted from unpublished CORAVEL velocities, yielding a drift of  $V_r(B)$  over 1975–1995.

**WDS 18070+3034AB.** Based on available CORAVEL velocities (unpublished measurements are given in Table A.10), a combined astrometric/spectroscopic solution (Table A.2 and Fig. A.8) improves the spectroscopic orbital elements provided by Abt & Willmarth (2006) for that system. AC 15 AB is a triple system, with the separation Aa-Ab amounting to  $0.228''$  and that of AB to  $0.851''$  in 2005, according to Scardia et al. (2008).

**WDS 18428+5938AB.** Velocity measurements (4 for  $V_r(A)$  and one for  $V_r(B)$ ) obtained by the HERMES spectrograph in 2012 are listed in Table A.1.

**WDS 18570+3254AB.** A combined astrometric/spectroscopic solution confirms the spectroscopic orbital elements provided by

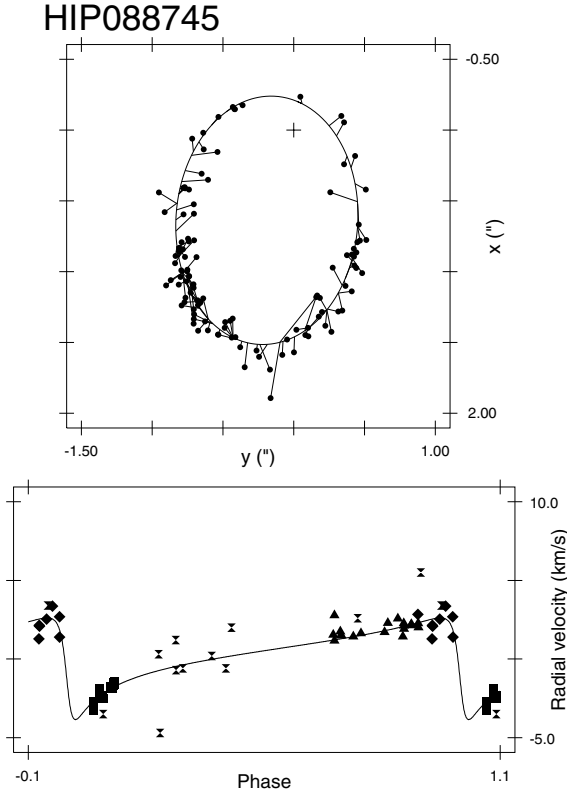


**Fig. A.8.** Combined astrometric (*upper panel*) and spectroscopic (*lower panel*) orbit for WDS 18070+3034AB. The solid line in the lower panel corresponds to the predicted velocity curve for A. Individual measurements for the visual orbit were taken from the WDS database at USNO. In the lower panel, triangles correspond to CORAVEL data, squares to velocities from [Abt & Willmarth \(2006\)](#), diamonds to [Tokovinin & Smekhov \(2002\)](#), and double triangles to the old radial velocities collected by [Kamper & Beardsley \(1986\)](#).

[Abt & Willmarth \(2006\)](#) for that system. BU 648 AB is a binary with an exoplanet ([Muterspaugh et al. 2010c](#)) in coplanar orbits. WDS 19121+0254AB. Masses are from [Benedict et al. \(2001\)](#). WDS 19255+0307Aa,Ab. [Kamper et al. \(1989\)](#) performed a combined spectroscopic/astrometric analysis of the Aa-Ab pair. We adopted the orbital elements from their Table V, except that  $180^\circ$  was added to their value of  $\omega$ , to conform with our convention that  $\omega$  corresponds to the visual orbit of Ab around Aa, rather than to the spectroscopic orbit of Aa around the centre of mass. One HERMES measurement was obtained (Table A.1) that reveals for the first time the companion in the cross-correlation function as a narrow peak on top of the broad peak ( $V_r \sin i = 84 \text{ km s}^{-1}$ ) due to the FV primary (Fig. A.9). The companion does not rotate fast. From the orbit described in [Kamper et al. \(1989\)](#), we estimate that the HERMES data point ( $V_r(\text{Aa}) = -26.68 \text{ km s}^{-1}$ ) has been taken at orbital phase  $0.54 \pm 0.14$ , when the velocity is  $1.66 \pm_{0.70}^{0.15} \text{ km s}^{-1}$  higher than the centre of mass (CoM) velocity. The CoM velocity is thus estimated to be  $-28.34 \pm_{0.70}^{0.15} \text{ km s}^{-1}$ . Combined with  $V_r(\text{Ab}) = -37.70 \text{ km s}^{-1}$ , this yields a surprisingly high mass ratio  $M_{\text{Aa}}/M_{\text{Ab}}$  of 5.6, or a mass of  $0.29 M_\odot$  for the companion if the primary is a F0V star of mass  $1.6 M_\odot$ . The corresponding spectral type would then be M4V for the Ab component, 8.6 mag fainter than the primary component. The close pair WDS 19255+0307Aa,Ab, seems to form a triple system with the wide pair (WDS 19255+0307AB = BUP 190, separation 96

**Table A.4.** CORAVEL velocities (labelled C in the last column), [Tokovinin & Smekhov \(2002\)](#) velocities (labelled T), and [Chubak et al. \(2012\)](#) velocities (labelled M) for the AB components of WDS 00057+4549AB = HIP 473.

JD - 2 400 000	$V_r$ A ( $\text{km s}^{-1}$ )		$V_r$ B ( $\text{km s}^{-1}$ )		$V_r$ B-A ( $\text{km s}^{-1}$ )	
43 791.437	1.83	0.43	-1.99	0.46	-3.82	C
43 791.450	1.16	0.48	-1.95	0.49	-3.11	C
43 795.447	1.45	0.43	-1.59	0.47	-3.04	C
43 806.403	1.16	0.43	-1.92	0.53	-3.08	C
43 808.388	1.32	0.43	-1.74	0.53	-3.06	C
43 813.391	0.19	0.51	-1.41	0.52	-1.60	C
44 211.319	0.67	0.47	-0.35	0.61	-1.02	C
44 849.517	1.48	0.45	-2.26	0.45	-3.74	C
45 264.406	1.06	0.37	-1.91	0.36	-2.97	C
45 615.458	1.63	0.48	-2.57	0.46	-4.20	C
46 008.457	1.86	0.48	-1.99	0.53	-3.87	C
46 016.404	1.12	0.56	-2.81	0.54	-3.93	C
46 372.418	0.85	0.33	-2.53	0.50	-3.38	C
46 373.385	0.87	0.34	-2.69	0.44	-3.56	C
46 413.273	0.96	0.43	-2.84	0.48	-3.80	C
46 725.421	0.87	0.52	-2.55	0.58	-3.42	C
47 035.584	1.01	0.50	-2.18	0.51	-3.19	C
47 556.262	-0.01	0.39	-2.14	0.40	-2.13	C
47 733.622	0.12	0.54	-1.13	0.58	-1.25	C
47 853.376	1.17	0.48	-1.54	0.56	-2.71	C
48 119.635	0.66	0.38	-2.44	0.39	-3.10	C
48 237.300	0.72	0.39	-1.91	0.37	-2.63	C
48 495.535	0.81	0.38	-2.39	0.38	-3.20	C
48 571.438	0.87	0.31	-2.54	0.40	-3.41	C
48 860.589	0.66	0.50	-2.74	0.51	-3.40	C
49 036.326	0.58	1.07	-	-	-	C
49 592.549	0.37	0.37	-2.43	0.35	-2.80	C
49 598.459	1.43	0.40	-1.96	0.39	-3.39	C
49 950.579	0.20	0.57	-4.64	0.59	-4.84	C
49 975.449	0.34	0.24	-2.30	0.25	-2.64	T
50 324.457	0.06	0.34	-	-	-	T
50 341.514	1.73	0.46	-3.97	0.51	-5.70	C
50 650.553	1.57	0.27	-3.06	0.34	-4.63	T
50 658.553	0.63	0.42	-2.46	0.56	-3.09	T
50 667.570	2.76	0.73	-1.12	0.63	-3.88	T
50 758.298	0.21	0.54	-0.87	0.52	-1.08	T
51 065.517	2.00	0.32	-1.92	0.26	-3.92	T
54 172.5	1.654	0.14	-1.700	0.10	-3.35	M

to  $133''$ ), but the physical nature of this system is yet to be confirmed.

WDS 21000+4004AB. [Fekel et al. \(1978\)](#) found that the visual component A of KUI 103 is itself a spectroscopic binary with a period of 3.27 d, but no information is available about coplanarity ([Tokovinin 2008](#)). [Pourbaix \(2000\)](#) has made a combined analysis of the visual and spectroscopic data. However, the authors note that this orbital solution is somewhat uncertain, given the large error bars and inconsistencies in the derived values for stellar masses and orbital parallax. Thus, we decided to base our determination of the orbital pole of this system on the analysis of the published radial velocity measurements ([Pourbaix 2000](#)) and the orbital elements of the new visual orbit proposed by [Docobo & Ling \(2010\)](#).

WDS 21069+3845AB. The mass ratio is taken from [Gorshanov et al. \(2006\)](#). The node assignment is based on the difference  $V_r(\text{B}) - V_r(\text{A}) \sim +1 \text{ km s}^{-1} > 0$ , as provided by Table 1

**Table A.5.** CORAVEL velocities for the components of WDS 01083+5455Aa,Ab =  $\mu$  Cas.

Date	JD - 2 400 000	$V_r$ (km s <sup>-1</sup> )	
210877	43 377.577	-99.42	0.56
050977	43 392.532	-99.72	0.41
050977	43 392.535	-99.88	0.49
070977	43 394.540	-99.64	0.45
070977	43 394.542	-99.49	0.41
170977	43 404.505	-100.03	0.51
170977	43 404.509	-100.77	0.52
171077	43 434.481	-99.30	0.47
171077	43 434.483	-99.32	0.45
011177	43 449.431	-99.21	0.62
011177	43 449.435	-99.07	0.48
011177	43 449.435	-99.07	0.48
011177	43 449.438	-99.37	0.51
191177	43 467.378	-98.83	0.39
191177	43 467.381	-98.76	0.39
191177	43 467.383	-99.29	0.44
180878	43 739.617	-99.13	0.37
190878	43 740.621	-99.32	0.34
240878	43 745.611	-98.91	0.33
240878	43 745.615	-99.38	0.33
211078	43 803.444	-100.06	0.35
081083	45 616.487	-97.44	0.35
240984	45 968.530	-97.42	0.34
070885	46 285.624	-96.88	0.35
201285	46 420.266	-96.47	0.37
020886	46 645.615	-96.48	0.32
300886	46 673.600	-96.73	0.36
021086	46 706.588	-96.62	0.36
071286	46 772.252	-96.37	0.37
111286	46 776.302	-96.50	0.36
170287	46 844.400	-96.44	0.33
121088	47 447.622	-95.83	0.37
170889	47 756.617	-96.46	0.36
170890	48 121.622	-96.12	0.36
141290	48 240.385	-96.06	0.36
200892	48 855.626	-96.27	0.35
250193	49 013.283	-96.23	0.36
180893	49 218.623	-95.90	0.33
200194	49 373.279	-96.39	0.35
080994	49 604.572	-97.11	0.35
200895	49 950.602	-97.12	0.44
130996	50 340.559	-98.85	0.36
120897	50 673.624	-100.58	0.39
090198	50 823.228	-100.67	0.32
200199	51 199.245	-99.14	0.34

**Table A.6.** New CORAVEL velocities for the components of WDS 01418+4237AB in complement of velocities published by Duquennoy & Mayor (1991).

Date	JD - 2 400 000	$V_r$ (km s <sup>-1</sup> )	
160890	48 120.647	4.12	0.33
070990	48 142.581	4.31	0.33
050891	48 474.627	3.32	0.32
240891	48 493.570	3.44	0.30
180892	48 853.646	2.64	0.32
250193	49 013.276	2.91	0.32
180893	49 218.649	2.14	0.32
200194	49 373.273	1.86	0.31
080994	49 604.602	0.87	0.32
190895	49 949.643	-0.27	0.38
130996	50 340.573	-0.64	0.33
090198	50 823.239	1.06	0.32
200199	51 199.263	3.04	0.32

**Table A.7.** CORAVEL velocities for the components of WDS 02278+0426AB.

Date	JD - 2 400 000	$V_r(2)^a \pm$ (km s <sup>-1</sup> )		$V_r(1) \pm$ (km s <sup>-1</sup> )	
011078	43 783.569	9.67	0.67	4.65	0.73
281078	43 810.476	9.11	0.86	4.81	0.96
301078	43 812.523	8.38	1.04	3.89	1.17
120279	43 917.269	9.28	0.73	4.76	0.81
180280	44 288.279	10.17	0.64	4.52	0.70
051081	44 883.540	11.13	0.66	3.65	0.72
281082	45 271.562	11.28	0.57	1.49	0.62
061083	45 614.559	13.10	0.58	1.45	0.63
011084	45 975.561	14.07	0.63	1.72	0.69
111185	46 381.452	13.86	0.68	-0.18	0.75
300986	46 704.567	13.03	0.62	0.46	0.67
270887	47 035.618	12.19	0.61	2.28	0.67
201088	47 455.516	10.78	0.61	2.66	0.67
231189	47 854.441	8.69	0.50	3.96	0.53
040990	48 139.643	5.24	0.83	7.94	0.75
061191	48 567.490	3.26	0.66	10.93	0.72
240892	48 859.605	2.30	0.62	11.08	0.67
050992	48 871.837	4.17	0.60	9.25	0.65
210193	49 009.264	2.07	0.51	10.97	0.54
180293	49 037.264	2.36	1.18	11.02	1.33
081293	49 330.432	1.82	0.54	10.70	0.58
280894	49 593.912	3.82	0.58	6.69	0.63
080994	49 604.626	1.39	0.54	10.35	0.57
240895	49 954.651	0.79	0.71	12.15	0.78
120996	50 339.632	0.75	0.68	11.82	0.75
090198	50 823.312	2.10	0.56	10.35	0.60
150199	51 194.289	2.74	0.57	10.18	0.62

**Notes.** <sup>(a)</sup> Most likely, spectroscopic component 2 is WDS 02278+0426B (see text for details).

of Gorshanov et al. (2006) and confirmed by unpublished CORAVEL measurements.

WDS 22234+3228AB. The total mass seems too high for the spectral type.

WDS 22280+5742AB. Masses are from Delfosse et al. (2000). Among the many radial velocities available in the literature for the components of this system, we give the highest weight to the measurement [ $V_r(A) = -32.7$  km s<sup>-1</sup> and  $V_r(B) = -33.2$  km s<sup>-1</sup>] by Gizis et al. (2002) because (i) that measurement is precisely dated (JD 2 450 005.6) and on the same night for A and B; and (ii) the 0.5 km s<sup>-1</sup> velocity difference is consistent

with the prediction from the visual orbit. The measurement ( $V_r(A) = -34.0$  km s<sup>-1</sup> and  $V_r(B) = -35.0$  km s<sup>-1</sup>) by Delfosse et al. (1998) is equally useful (its epoch is not as precisely known as that report by Gizis, but it was obtained between September 1995 and March 1997, a short time span with respect to the 44.7 yr orbital period); the 1 km s<sup>-1</sup> velocity difference agrees better with the prediction from the visual orbit than Gizis' 0.5 km s<sup>-1</sup>. The determination of the *sign* of  $V_r(B) - V_r(A) = -1$  km s<sup>-1</sup> is important and it is opposite to the

**Table A.8.** New CORAVEL velocities for the components of WDS 16413+3136AB in complement of velocities published by Duquennoy & Mayor (1991).

Date	JD-2 400 000	$V_r$ ( $\text{km s}^{-1}$ )	
270490	48 009.500	-68.18	0.32
090891	48 478.459	-67.56	0.32
070592	48 750.578	-67.49	0.32
020393	49 049.692	-67.57	0.31
140494	49 457.592	-66.77	0.33
140797	50 644.431	-67.76	0.33

**Table A.9.** New CORAVEL velocities for the components of WDS 17121+4540AB.

Date	JD - 2 400 000	$V_r$ ( $\text{km s}^{-1}$ )	
200477	43 254.623	-83.29	0.42
220477	43 256.617	-31.08	0.71
220477	43 256.633	-32.85	0.88
130378	43 581.648	-28.31	0.66
130378	43 581.662	8.83	0.93
270678	43 687.480	-26.94	1.10
180778	43 708.394	-27.87	1.11
210778	43 711.380	-29.76	0.73
220778	43 712.391	-29.06	0.68
240778	43 714.428	-28.50	0.68
140679	44 039.489	-29.18	0.93
140879	44 100.355	-29.56	0.68
010981	44 849.362	-30.13	0.84
250282	45 026.692	-30.34	0.76
160583	45 471.566	-31.33	0.57
300384	45 790.675	-30.06	0.73
280784	45 910.384	-30.68	0.52
130385	46 138.686	-30.11	0.77
110586	46 562.568	-30.74	0.72
200787	46 997.453	-30.82	0.63
230388	47 244.665	-31.06	0.61
070788	47 350.452	-30.88	0.52
060689	47 684.589	-31.15	0.46
270490	48 009.538	-32.24	0.71
190890	48 123.457	-31.65	0.71
070791	48 445.443	-28.81	0.68
051191	48 566.246	-29.53	0.64
080592	48 751.570	-30.31	0.66
190892	48 854.345	-29.40	0.60
210493	49 099.595	-30.22	0.53
140494	49 457.583	-29.35	0.51
260895	49 956.360	-31.26	0.65
110596	50 215.561	-29.70	0.50
140797	50 644.441	-30.55	0.47
070598	50 941.589	-30.94	0.46

prediction from the visual orbital elements from the 6th COVBS. It is thus necessary to add  $180^\circ$  to the values of  $\Omega$  and  $\omega$  listed in the 6th COVBS. It is noteworthy that the velocity values listed in the Wilson – Evans – Batten catalogue (Duflot et al. 1995,  $V_r(A) = -24.0 \text{ km s}^{-1}$  and  $V_r(B) = -28.0 \text{ km s}^{-1}$ ) or in Reid et al. (1995) ( $V_r(A) = -16.0 \text{ km s}^{-1}$  and  $V_r(B) = -29.0 \text{ km s}^{-1}$ ), although the differences are much larger than anticipated, always have  $V_r(B) - V_r(A) < 0$ .

WDS 23317+1956AB. Indeterminate visual orbit.

WDS 23524+7533AB. Indeterminate visual orbit. A triple system with A being SB2 with a period of 7.75 d (Christie 1934).

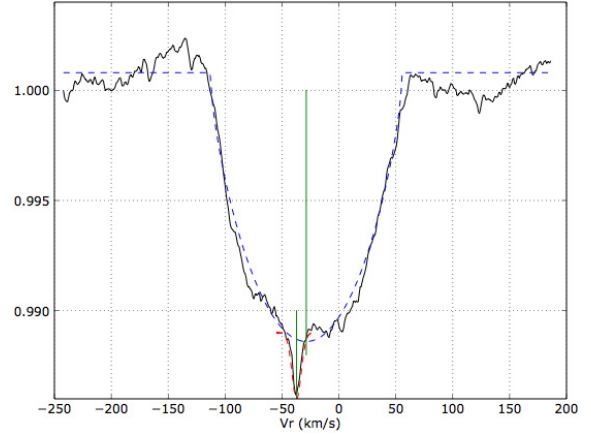


**Fig. A.9.** Cross-correlation function of the HERMES spectrum of WDS 19255+0307Aa,Ab (obtained at JD 2455 657.742) with a F0V template. Component Aa shows a rotationally broadened profile with  $V_r \sin i = 84 \text{ km s}^{-1}$ , and component Ab is visible as a weak Gaussian (at  $V_r(\text{Ab}) = -37.70 \text{ km s}^{-1}$ ) superimposed on the rotationally broadened profile (centred on  $V_r(\text{Aa}) = -26.68 \text{ km s}^{-1}$ ). Similar profiles have been observed over several consecutive nights.

**Table A.10.** New CORAVEL velocities for the components of WDS 18070+3034AB in complement of velocities published by Duquennoy & Mayor (1991).

Date	JD - 2 400 000	$V_r$ ( $\text{km s}^{-1}$ )	
190790	48 092.429	2.15	0.32
180890	48 122.388	2.21	0.33
020891	48 471.433	2.27	0.33
210891	48 490.384	2.02	0.32

## Appendix B: Determining the orbital pole of a double star

### B.1. Orbital pole of a visual double star

The true relative orbit (B/A) is related to the classical visual orbit of B relative to A. The pole of this orbit is defined by the unit vector perpendicular to the orbital plane and directed in such a way that an observer placed at its end sees that the B component has a direct motion (counter-clockwise).

The spatial motion of the binary components is described using the reference frame (A,  $x$ ,  $y$ ,  $z$ ) centred on the A component with two axes in the plane tangent to the celestial sphere (which is denoted plane of the sky):  $Ax$  points north (position angle =  $0^\circ$ ),  $Ay$  points east (position angle =  $90^\circ$ ), and the third axis  $Az$  is along the line of sight, pointing in the direction of increasing radial velocities (i.e. positive radial velocity). This reference frame is thus retrograde (i.e., viewed from the positive side of the  $Az$ -axis, a rotation of the  $Ax$ -axis onto the  $Ay$ -axis is carried out clockwise).

The relative (B/A) orbit is described by means of seven orbital elements:

- (i) Four so-called dynamic elements specifying the properties of the Keplerian motion in the true orbit ( $T$ , the epoch of passage through periastron;  $P$ , the revolution period;  $a$ , the semi-major axis and  $e$ , the eccentricity).

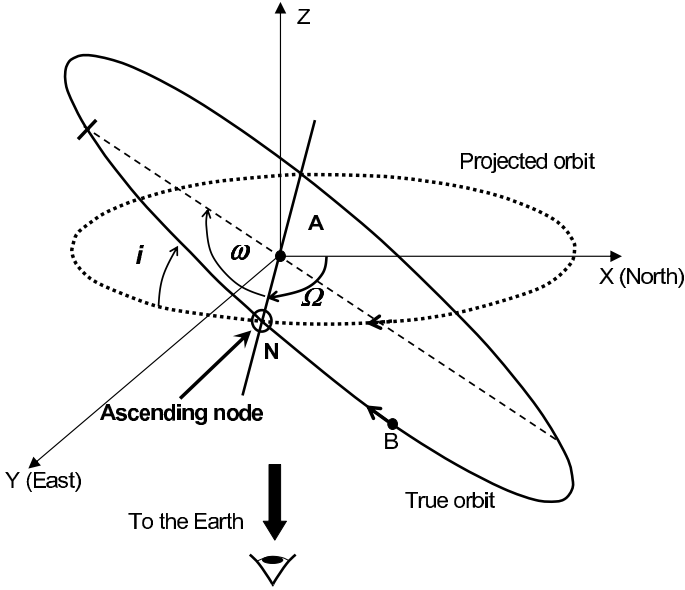


**Fig. B.1.** True and the projected relative orbit (B/A) of a visual binary and its geometrical elements. The ascending node of the orbit is located at point N.

(ii) Three so-called geometric elements that define the orientation of the true and apparent orbits, the latter being the projection of the true orbit on the plane of the sky (see Fig. B.1):

- $\Omega$  is the position angle of the line of intersection between the true orbital plane and the plane of the sky. There are two nodes whose position angles differ by  $180^\circ$ , but by convention,  $\Omega$  is the position angle of the ascending node where the orbital motion is directed away from the Sun. If radial-velocity measurements are not available to identify the ascending node, a temporary value ranging between  $0^\circ$  and  $180^\circ$  is adopted (Finsen 1934).
- $i$ , the inclination, is the angle between the planes of the projected orbit and of the true orbit, taken at the ascending node. The motion is direct if  $0^\circ < i < 90^\circ$  and retrograde if  $90^\circ < i < 180^\circ$ .
- $\omega$  is the argument of the periastron in the true orbit plane, measured in the direction of the orbital motion from the ascending node with a value ranging from  $0^\circ$  to  $360^\circ$ .

Two other orbits may be considered: the (A/AB) orbit of A around the centre of mass AB and the (B/AB) orbit of B around the centre of mass.

For resolved binaries, astrometric observations give then access to the (A/AB) and (B/AB) orbits projected on the plane of the sky. For an unresolved binary, the astrometric measurements capture the position of the photocentre F located between A and AB. The astrometric orbit (F/AB) is similar to that of (A/AB), but with a smaller semi-major axis  $a_F$ .

For a given projected orbit as derived from astrometric observations, two possible true orbits correspond that are symmetric with respect to the plane of the sky.

Therefore, even though the dynamic elements and the inclination  $i$  are determined unambiguously, it is impossible to select between the two possible true orbits (and thus between the two possible ascending nodes  $\Omega$ ) without a radial-velocity measurement. The argument of periastron  $\omega$  being measured from the ascending node, the ambiguity on  $\Omega$  thus propagates onto  $\omega$ . One special case is  $i = 0^\circ$  or  $180^\circ$ , the true orbit being then in the plane of the sky, and there is no ambiguity on the ascending node

(since there is no such thing as an ascending node in that case!). In all other cases, radial-velocity measurements for at least one component are needed to lift the ambiguity on the value of  $\Omega$ , before the orientation of the orbital pole can be fixed, as was done by Dommanget (2005) and Dommanget & Nys (2006).

## B.2. Radial velocities

If  $V_r(A)$ ,  $V_r(B)$  and  $V_{r,\text{sys}}$  are the heliocentric radial velocities of components A and B and of the centre of mass of the binary AB, and denoting  $V_{A/AB}$  and  $V_{B/AB}$  the radial components of the orbital velocity of A and B around the centre of mass, then

$$V_r(A, B) = V_{(A,B)/AB} + V_{r,\text{sys}}. \quad (\text{B.1})$$

The orbital radial velocity of each component relates to the orbital elements by

$$V_{(A,B)/AB} = 2\pi \frac{a_{(A,B)} \sin i}{P \sqrt{1 - e^2}} [e \cos \omega_{(A,B)} + \cos(\omega_{(A,B)} + v)], \quad (\text{B.2})$$

where  $v$  is the true anomaly,  $a_{A,B}$  are the semi-major axes,  $P$  the orbital period, and  $\omega_{(A,B)}$  the argument of the periastron of the (A/AB) and (B/AB) orbits.

For double-lined spectroscopic binaries (SB2), the measurements of  $V_{A/AB}$  and  $V_{B/AB}$  are possible; for single-lined spectroscopic binaries (SB1), only  $V_{A/AB}$  measurements are possible.

The relative radial velocity between the components,  $V_r = V_r(B) - V_r(A)$ , can be calculated from the orbital elements of the (B/A) orbit using Eq. (B.2).

For an astrometric-binary orbit, the radial velocity of the photocentre  $V_r(F)$  can be computed with the same formula (Eq. (B.2)) where the semi-major axis  $a_F$  and the argument of the periastron  $\omega_F$  of the photocentric orbit have been inserted instead.

It is easy to show that

$$\omega_A = \omega_F = \omega_B + 180^\circ. \quad (\text{B.3})$$

The variation of  $V_r$  and  $V_r(B)$  are the same and are opposite to that of  $V_r(A)$ . By definition, the maximum of the  $V_r(A)$  and  $V_r(B)$  curves occurs at the passage of the ascending node in the true orbits (A/AB) and (B/AB), respectively, whereas the maximum of the  $V_r$  curve corresponds to the passage at the ascending node in the relative orbit (B/A).

## B.3. Choosing the correct ascending node

Generally, the ascending node  $\Omega$  of the relative orbit (B/A) is determined by comparing the variations of the measured radial velocities  $V_r$  with the shape of the relative radial-velocity curve  $\tilde{V}_r$  (or  $\tilde{V}_r(F)$ ) computed from the visual orbital elements. However, finding the ascending node of the relative orbit (B/A) in practice depends on the type of binary system and on the type of radial-velocity measurements available, as described in Table B.1.

For spectroscopic systems with a combined spectro-visual orbit available (case 1 of Table B.1), the ascending node of the relative orbit is unambiguously determined (e.g., Pourbaix 2000). The values of the orbital elements  $i$ ,  $\Omega$  and  $\omega$  can then be directly used to compute the orbital pole orientation.

For visual binaries with available radial-velocity measurements, if the slope of the computed  $\tilde{V}_r$  curve is the same as that of the  $V_r(B) - V_r(A)$  measurements (cases 2 or 5 of Table B.1), or opposite to that of the  $V_r(A)$  curve (cases 3 or 6 of Table B.1), there is no need to change the values of the position angle of the

**Table B.1.** The different ways to determine the ascending node of the relative orbit (B/A).

System type	Available orbit	Available velocities	Ascending node determination	Case
Spectroscopic binary	spectro-visual	from orbit	$i, \Omega, \omega$ result from (B/A) orbit computation	1
resolved as	visual and SB2	$V_r(\text{B}), V_r(\text{A})$ from orbit	$\tilde{V}_r(\text{B/A})$ compared to $V_r(\text{B})-V_r(\text{A})$	2
visual or astrometric	visual and SB1	$V_r(\text{A})$ from orbit	$\tilde{V}_{\text{AB/A}}$ compared to $V_r(\text{A})$	3
binary	astrometric and SB1	$V_r(\text{A})$ from orbit	$\tilde{V}_r(\text{F})$ compared to $V_r(\text{A})$	4
Visual binary	visual	$V_r(\text{A})$ and $V_r(\text{B})$	$\tilde{V}_r$ compared to $V_r(\text{B})-V_r(\text{A})$ drift	5
		$V_r(\text{A})$	$\tilde{V}_r$ compared to $V_r(\text{A})$ drift	6
Astrometric binary	astrometric	$V_r(\text{A})$	$\tilde{V}_r(\text{F})$ compared to $V_r(\text{A})$ drift	7

**Notes.** In the table, the  $\tilde{V}_r$  quantities denote the values derived from the visual or astrometric elements through Eq. (B.2), the values without a tilde are the observed values.

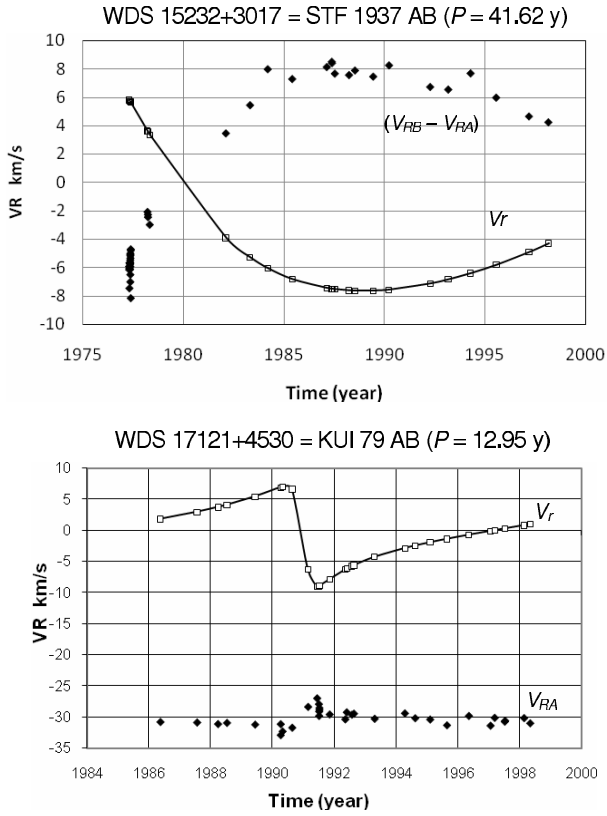


**Fig. B.2.** Examples of lifting the ambiguity on the ascending node for a visual binary. *Top* (cases 2, 5 of Table B.1): the slope of the computed  $\tilde{V}_r$  curve is opposite to that of the  $V_r(\text{B})-V_r(\text{A})$  measurements: it is then necessary to add  $180^\circ$  to the values of  $\Omega$  and  $\omega$  given by the 6th Catalog of Orbits of Visual Binary Stars (6th COVBS; Hartkopf et al. 2001). *Bottom* (cases 3, 6 of Table B.1): the slope of the computed  $\tilde{V}_r$  curve is opposite to that of  $V_r(\text{A})$  measurements; there is no need to change the values of  $\Omega$  and  $\omega$  listed in the 6th COVBS.

ascending node  $\Omega$  and of the argument of the periastron  $\omega$ , from the values adopted for computing  $\tilde{V}_r$  in Eq. (B.2). In the opposite situation, it is necessary to add  $180^\circ$  to the values of  $\Omega$  and  $\omega$ . Examples are given in Fig. B.2.

For astrometric binaries (cases 4 or 7 of Table B.1), if the drift of the computed  $\tilde{V}_r(\text{F})$  curve is opposite that of the  $V_r(\text{A})$  measurements, there will be no need to change the values of the

position angle of the ascending node  $\Omega_{\text{F}}$  or of the argument of the periastron  $\omega_{\text{F}}$ . In the opposite case, it is necessary to add  $180^\circ$  to these values. Thus the ascending node of the (B/A) orbit will be  $\Omega = \Omega_{\text{F}} + 180^\circ$  and  $\omega = \omega_{\text{F}} + 180^\circ$ .

It is important to note that the ambiguity-free values listed in Table 3 are correspond to the relative orbit (B/A). Hence, in Tables A.2 and A.3, which provide newly determined orbital elements of spectro-visual orbits, we list the values of  $\omega_{\text{B}}$ , contrary to usage with spectroscopic orbital elements, to ensure consistency with Table 3.

#### B.4. Determining the direction of the pole of the true relative orbit

This section describes the determination of the direction of the pole of the true relative orbit (B/A), including the case of astrometric binaries for which the B component is invisible.

In the reference frame  $(\text{A}, x', y', z')$  attached to the (B/A) orbit, the direction of the orbital pole is given by the unit vector  $(x', y', z') = (0, 0, 1)$ .

The ambiguity on the position angle of the ascending node was solved along the method described in Sect. B.3, the geometric orbital elements  $i, \Omega$  and  $\omega$  are known, so that the equatorial coordinates of the pole  $(x_{\text{eq}}, y_{\text{eq}}, z_{\text{eq}})$  can be computed from the equatorial coordinates of the binary (Right Ascension  $\alpha$ , Declination  $\delta$ ) by a succession of reference-frame changes as shown in Fig. B.3:

- From  $(\text{A}, x', y', z')$  to  $(\text{A}, x', u, z)$  by a rotation of angle  $i$  around the  $\text{Ax}'$  axis;
- to  $(\text{A}, x, y, z)$  by a rotation of angle  $\Omega$  around the  $\text{Az}$  axis;
- to  $(\text{O}, v, y, z_{\text{eq}})$  by a rotation of angle  $\delta$  around the  $\text{Ay}$  axis;
- and finally to  $(\text{O}, x_{\text{eq}}, y_{\text{eq}}, z_{\text{eq}})$  by a rotation of angle  $\alpha$  around the  $\text{Az}_{\text{eq}}$  axis.

It is then easy to show that in the equatorial reference frame  $(\text{O}, x_{\text{eq}}, y_{\text{eq}}, z_{\text{eq}})$ , the direction of the orbital pole is given by the unit vector with the coordinates

$$\begin{aligned} x_{\text{eq}} &= \cos \alpha \sin \delta \sin \Omega \sin i - \cos \alpha \cos \delta \cos i - \sin \alpha \cos \Omega \sin i \\ y_{\text{eq}} &= \sin \alpha \sin \delta \sin \Omega \sin i - \sin \alpha \cos \delta \cos i + \cos \alpha \cos \Omega \sin i \\ z_{\text{eq}} &= -\cos \delta \sin \Omega \sin i - \sin \delta \cos i. \end{aligned} \quad (\text{B.4})$$

We stress that our convention, which leads to a polar direction opposite to that of the system when  $i = 0^\circ$ , is opposite to that

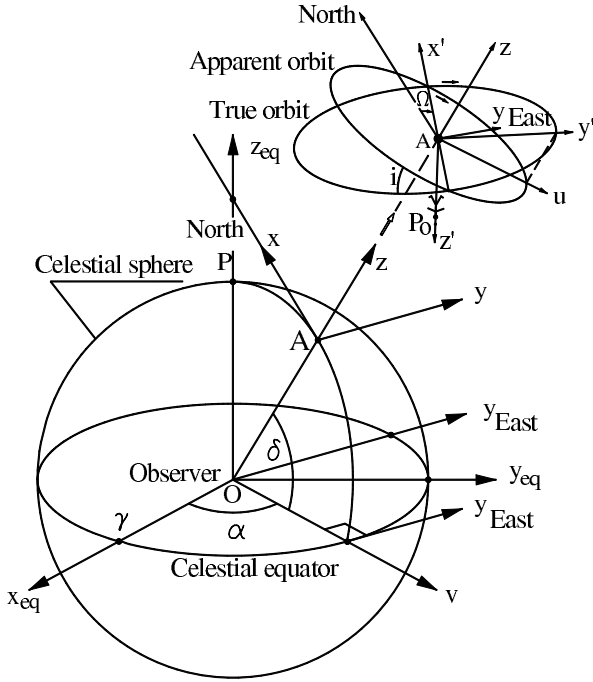


**Fig. B.3.** Orientation of the true and apparent relative orbits (B/A) with respect to the celestial sphere and the corresponding reference frames.  $(\alpha, \delta)$  are the equatorial coordinates of the binary system.

of [Batten \(1967\)](#). In the terminology of [Batten \(1967\)](#), our poles are thus those that would be derived by applying the right-hand rule to the orbital motion.

The Galactic coordinate system is the most appropriate for studying the distribution of the orbital poles in a Galactic framework. Therefore, the coordinates  $(x_{\text{eq}}, y_{\text{eq}}, z_{\text{eq}})$  of the unit vector giving the direction of the pole are converted into the coordinates  $(x_{\text{g}}, y_{\text{g}}, z_{\text{g}})$  in the Galactic frame using the relation (for details see [Johnson & Soderblom 1987](#))

$$\begin{pmatrix} x_{\text{g}} \\ y_{\text{g}} \\ z_{\text{g}} \end{pmatrix} = [T] \begin{pmatrix} x_{\text{eq}} \\ y_{\text{eq}} \\ z_{\text{eq}} \end{pmatrix}. \quad (\text{B.5})$$

The terms of the transformation matrix  $[T]$  are computed from the J2000 equatorial coordinates of the Galactic centre and pole given by the Institut de Mécanique Céleste et de Calcul des Ephémérides (IMCCE):

- North Galactic pole:  
 $\alpha_0 = 12^{\text{h}}51^{\text{m}}26.28^{\text{s}}$  and  $\delta_0 = 27^{\circ}7'41.7''$
- Galactic center:  
 $\alpha_{\text{G}} = 17^{\text{h}}45^{\text{m}}37.20^{\text{s}}$  and  $\delta_{\text{G}} = -28^{\circ}56'10.2''$

This leads to the transformation matrix:

$$[T] = \begin{pmatrix} -0.054875 & -0.873437 & -0.483835 \\ 0.494110 & -0.444829 & 0.746982 \\ -0.867666 & -0.198077 & 0.455984 \end{pmatrix}. \quad (\text{B.6})$$

After the coordinates  $(x_{\text{g}}, y_{\text{g}}, z_{\text{g}})$  are computed, the Galactic longitude  $l$  and latitude  $b$  are deduced using the relations

$$\begin{aligned} \cos l \cos b &= x_{\text{g}} \\ \sin l \cos b &= y_{\text{g}} \quad \text{with } 0^{\circ} \leq l < 360^{\circ} \\ \sin b &= z_{\text{g}} \quad \text{with } -90^{\circ} \leq b \leq 90^{\circ}. \end{aligned} \quad (\text{B.7})$$